# New insights into the Early Cambrian igneous and sedimentary history of the Arbuckle Mountains area of the Southern Oklahoma Aulacogen from basement well penetrations

**Robert E. Puckett, Jr.[1], Richard E. Hanson[2], Amy M. Eschberger[3], Matthew E. Brueseke[4], Casey L. Bulen[5], and Jonathan D. Price[6]**

*[1]12700 Arrowhead Lane, Oklahoma City, Oklahoma 73120. bpuckett@priceedwards.com. Corresponding author.*
*[2]School of Geology, Energy, and the Environment, Texas Christian University, Fort Worth, Texas 76129. r.hanson@tcu.edu.*
*[3]School of Geology, Energy, and the Environment, Texas Christian University, Fort Worth, Texas 76129. Current address: Colorado Department of Natural Resources, Division of Reclamation, Mining, and Safety, 1313 Sherman Street, Suite 215, Denver, Colorado 80203. aeschberger@yahoo.com.*
*[4]Department of Geology, Kansas State University, 108 Thompson Hall, Manhattan, Kansas 66506. brueseke@ksu.edu.*
*[5]Department of Geology, Kansas State University, 108 Thompson Hall, Manhattan, Kansas 66506. cabulen@gmail.com.*
*[6]Department of Chemistry, Geosciences, and Physics, Midwestern State University, 3410 Taft Boulevard, Wichita Falls, Texas 76308. jonathan.price@mwsu.edu.*

## GEOLOGIC FRAMEWORK

Partial inversion of the Southern Oklahoma Aulacogen occurred in the Late Pennsylvanian and was related either to the collisional Ouachita orogeny along the southern Laurentian margin or to far-field stresses transmitted inland from the Cordilleran margin to the west (Hanson et al., 2013). As first recognized by Ham et al. (1964), major Cambrian rift-bounding faults were reactivated to form reverse faults or thrusts in a compressional to transpressional regime (McConnell 1989; Perry, 1989). In the Arbuckle Mountains area of south-central Oklahoma, reactivation of the Washita Valley Fault resulted in the uplift and erosion of at least 7.3 km of Upper Cambrian through Middle Pennsylvanian sediments (Ham et al. 1964; Johnson et al., 1989), exposing rocks of the Lower Cambrian volcanic floor of the rift along the axis of the Arbuckle Anticline. The volcanic rocks are generally unconformably overlain by the Upper Cambrian Reagan Sandstone, which represents the basal unit in the Sauk Sequence transgression onto the rift and adjacent craton (Johnson et al., 1988).

In the western Arbuckles, Pennsylvanian reactivation of the north-vergent Washita Valley Fault resulted in Lower Cambrian igneous rocks being thrust over younger oil-bearing sedimentary rocks. Local deformation in the footwall of the fault trapped hydrocarbons in structurally complex Paleozoic sedimentary rocks and necessitates borehole penetration through overthrust igneous rocks to reach the underlying reservoirs. Beginning in the central Arbuckles and proceeding along a band 39 km long parallel to the northwest-striking fault, 40 wells penetrate the fault-truncated igneous section of the overthrust (Fig.1). Most were drilled in the early 1950's to 1960's, with the most recent one being drilled in 2001. These wells provide a wealth of information on parts of the volcanic succession, related intrusive rocks, and overlying strata not exposed in outcrop. In this report, we follow standard procedure in Oklahoma in referring to wells penetrating the Cambrian igneous rocks of the aulacogen as basement wells, but none of the wells reached older Proterozoic crust beneath the Cambrian igneous section.

## TECHNIQUES

Drill cuttings for the igneous section from 21 wells in the Arbuckle area (Table 1) have been examined. Lithologic logs for these wells are displayed in Figure 2, which represents a distance of 35 km northwest to southeast and generally parallel to the Washita Valley Fault. The horizontal datum used in Figure 2 is the unconformity surface separating the volcanic rocks from the overlying Reagan Sandstone or younger strata where the Reagan is absent. The only exception is the Frankfort 1 Sparks Ranch well, where the datum is taken as the base of an anomalous post-volcanic sedimentary sequence that predates typical Reagan Sandstone, as discussed below. The scale in Figure 2 refers to the thickness beneath the post-volcanic unconformity.

TABLE 1. INFORMATION FOR WELLS SHOWN IN FIGURE 2.

| Figure 2 Well # | Operator | Lease | Well # | Quarter | Sec. | T | | R | | Year Completed | Total Depth (ft) | Basement Depth (ft) | Basement Penetration (ft) | Basement Penetration (m) |
|---|---|---|---|---|---|---|---|---|---|---|---|---|---|---|
| 1 | L E JONES | NEWBERRY | 1 | S2 N2 NW SW | 13 | 1 | N | 3 | W | 1981 | 8782 | 2280 | 5053 | 1540.1544 |
| 2 | PAN AM | NEWBERRY UNIT | 1 | E2 NW NE NW | 24 | 1 | N | 3 | W | 1970 | 10741 | 1802 | 8938 | 2724.3024 |
| 3 | PAN AM | RINGER UNIT B 1 | 1 | NW NE SW SE | 13 | 1 | N | 3 | W | 1968 | 9445 | 2437 | 4877 | 1486.5096 |
| 4 | PAN AM | STORY 4 | 1 | NE SW SW | 18 | 1 | N | 2 | W | 1965 | 8200 | 4215 | 2025 | 617.22 |
| 5 | COHO | STORY 4 | 4 | SE NE SW SW | 18 | 1 | N | 2 | W | 2001 | 8000 | 4115 | 2585 | 787.908 |
| 6 | PAN AM | PICKETT UNIT B | 1-A | SE SW SE | 18 | 1 | N | 2 | W | 1963 | 8590 | 6010 | 427 | 130.1496 |
| 7 | PAN AM | JARMAN | 1-19 | C NE NW NE | 19 | 1 | N | 2 | W | 1964;1998 | 9321 | 3178 | 3675 | 1120.14 |
| 8 | PAN AM | WILLIAMS UNIT D 1 | 1 | SW NW | 20 | 1 | N | 2 | W | 1963 | 9567 | 3440 | 4455 | 1357.884 |
| 9 | PAN AM | S E EOLA BROMIDE | 13 | NE NE SE NE | 20 | 1 | N | 2 | W | 1970 | 9396 | 5520 | 800 | 243.84 |
| 10 | PAN AM | WILLIAMS UNIT C 1 | 1 | N2 N2 NW | 20 | 1 | N | 2 | W | 1963 | 9070 | 5598 | 492 | 149.9616 |
| 11 | NEWKUMET | WILLIAMS 1-20 | 1-20 | NW NE SW | 20 | 1 | N | 2 | W | 1998 | 9106 | 3720 | 4300 | 1310.64 |
| 12 | PAN AM | WILLIAMS UNIT D 2 | 2 | C NE SE NW | 20 | 1 | N | 2 | W | 1963 | 9085 | 3966 | 2874 | 875.9952 |
| 13 | PAN AM | WILLIAMS UNIT G 1 | 1 | C NE SW NE | 20 | 1 | N | 2 | W | 1964 | 8718 | 4720 | 1618 | 493.1664 |
| 14 | PAN AM | MOORE UNIT B | 1-A | SE NE | 20 | 1 | N | 2 | W | 1964 | 9416 | 5250 | 1680 | 512.064 |
| 15 | PAN AM | WHYTE UNIT 1 | 1 | SE NE SW | 21 | 1 | N | 2 | W | 1964 | 9396 | 4520 | 3125 | 952.5 |
| 16 | BOSWELL ENERGY CO. | YEARY | 1-22 | NE SW SW | 22 | 1 | N | 2 | W | 1985;1986 | 8922 | 6034 | 1306 | 398.0688 |
| 17 | UNION OIL CO. OF CAL. | MORTON | 1-31 | NE SW NE | 31 | 1 | N | 1 | W | 1984 | 16610 | 7260 | 5288 | 1611.7824 |
| 18 | JOHN A TAYLOR | MORROW | 1 | C S2 N2 SE | 32 | 1 | N | 1 | W | 1980 | 16123 | 6830 | 5790 | 1764.792 |
| 19 | FRANKFORT OIL CO. | SPARKS RANCH | 1 | C SE SE | 32 | 1 | S | 1 | W | 1956 | 12884 | 6820 | 6064 | 1848.3072 |
| 20 | HAMILTON BROS. OIL CO. | TURNER FALLS | 1-18A | SE NE NW SW | 18 | 1 | S | 1 | E | 1982 | 18500 | 200 | 15800 | 4815.84 |
| 21 | KAISER FRANCIS OIL CO. | CHAPMAN | 1 | NE SW SW | 9 | 2 | S | 2 | E | 1980 | 7677 | 1340 | 6337 | 1931.5176 |
| | | | | | | | | | | | | | **87509** | **26672.7432** |

The wells shown in Table 1 and Figure 2 penetrated 150 m to 4816 m of igneous rocks. In most of these wells the base of the igneous section is truncated by the Washita Valley Fault, except for several wells that stopped drilling in the igneous section. The samples for these wells are housed at the Oklahoma Petroleum Information Center (Oklahoma Geological Survey) in Norman, Oklahoma. The cuttings were collected during drilling operations at 3.05 m (10 ft) intervals, and the total igneous section examined in the present study is 26.67 km. The cuttings for some of the other wells drilled along this trend are not available, penetrated insufficient igneous section to be relevant, or were drilled after 2000; in the latter cases, newly developed, rapid drilling techniques have yielded very poor sample quality. All thicknesses shown are apparent drilled thickness. One well, the Hamilton Brothers 1-18A Turner Falls, ran a dipmeter log over the lower volcanic section, and the subsurface dips in that well are similar to the measured surface dips of 30° to 40°. These dips would result in an approximate 20% shortening in true thickness over drilled thickness. Dipmeter logs are not available for the other wells, and younger cover makes it impossible to obtain dips from the deformed Paleozoic sedimentary rocks in the areas where those wells occur.

Although subsurface techniques cannot produce the wealth of information derived from high-resolution surface mapping, a more complete section can be examined and certain features are readily discernible. Gamma-ray (GR) well logs, which measure radiation primarily from U, Th, and K, are extremely useful in distinguishing contacts between mafic and felsic volcanic and intrusive rocks in the bimodal Wichita Province. Some of the wells pre-date the use of GR logs, but many GR logs are available and were used in igneous stratigraphic interpretation (Fig. 3). Lithology cannot be determined using GR logs alone. For example, extrusive basalt cannot be distinguished from intrusive diabase, and rhyolite lava cannot be distinguished from granite or rhyolitic volcaniclastic rocks. However, examination of cuttings under a binocular microscope can typically distinguish these rock types.

Rhyolite flow boundaries may be identified using several criteria. The first is an abrupt change in texture with depth. This can be complicated by the presence of felsic hypabyssal intrusions, but these intrusions are generally a relatively bright orange-gray, the same color as seen in outcrops of similar intrusions exposed in the Arbuckles (Eschberger, 2012; Eschberger et al. paper, this guidebook). Ancient weathering surfaces tend to be well preserved in the subsurface, and the presence of an upper weathered in-

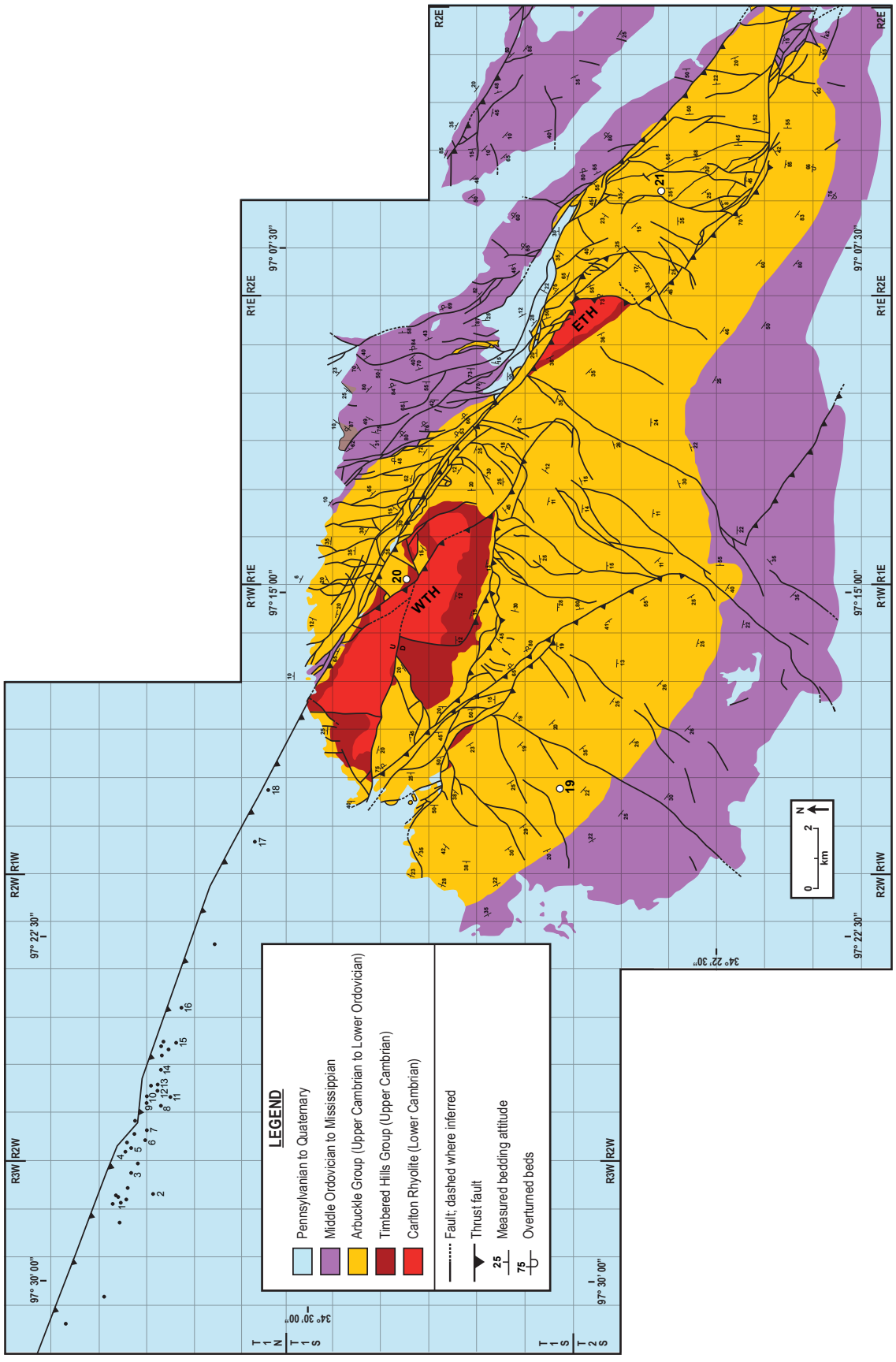


**Figure 1. Map of wells penetrating the igneous section of the Southern Oklahoma Aulacogen in the western Arbuckle Mountains area. Information on numbered wells is given in Table 1; locations of wells 19, 20, and 21 are indicated by white circles on Arbuckle map; WTH = West Timbered Hills; ETH = East Timbered Hills. Arbuckle map is modified from Johnson (1990).**

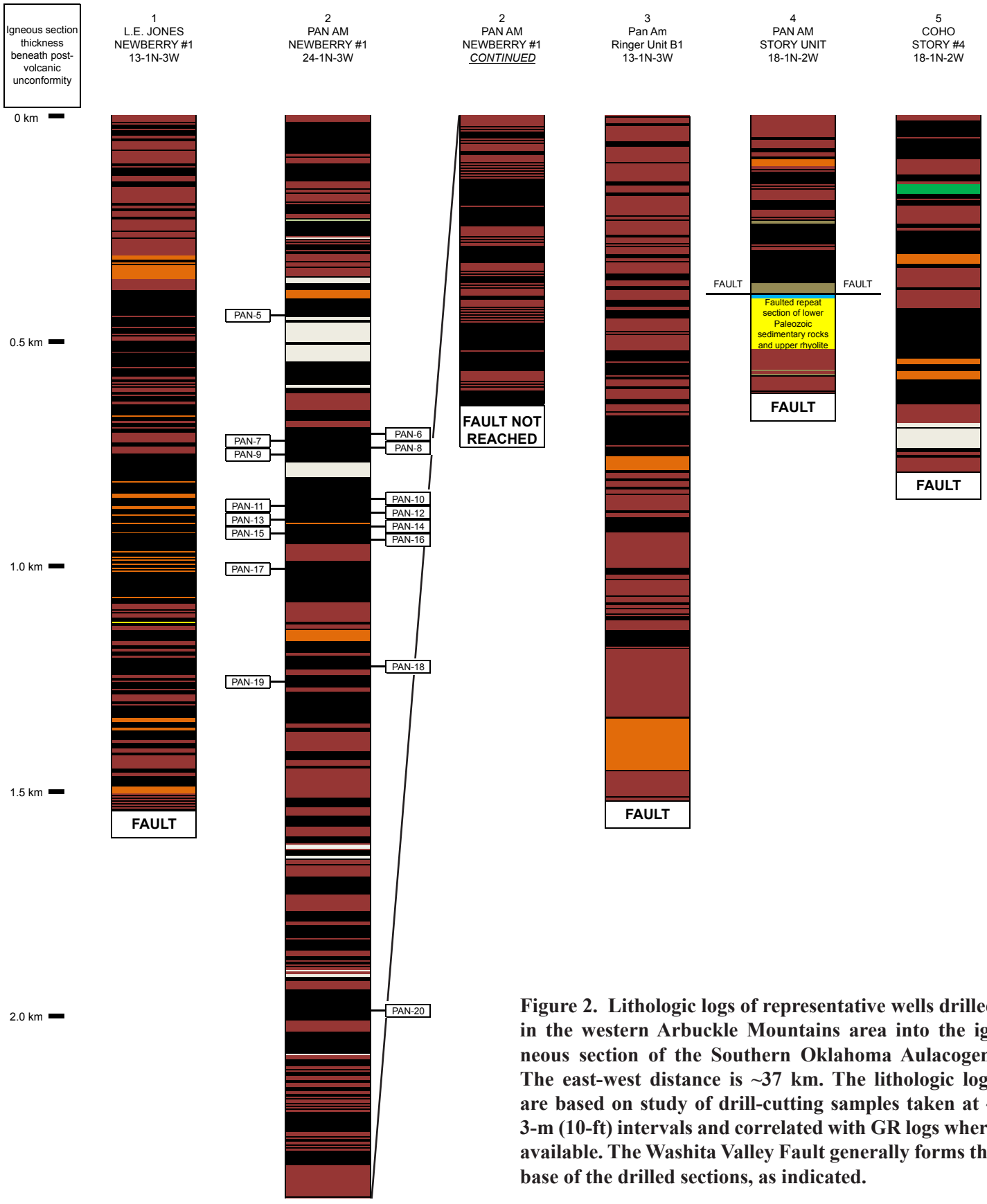


**Figure 2. Lithologic logs of representative wells drilled in the western Arbuckle Mountains area into the igneous section of the Southern Oklahoma Aulacogen. The east-west distance is ~37 km. The lithologic logs are based on study of drill-cutting samples taken at ~ 3-m (10-ft) intervals and correlated with GR logs where available. The Washita Valley Fault generally forms the base of the drilled sections, as indicated.**

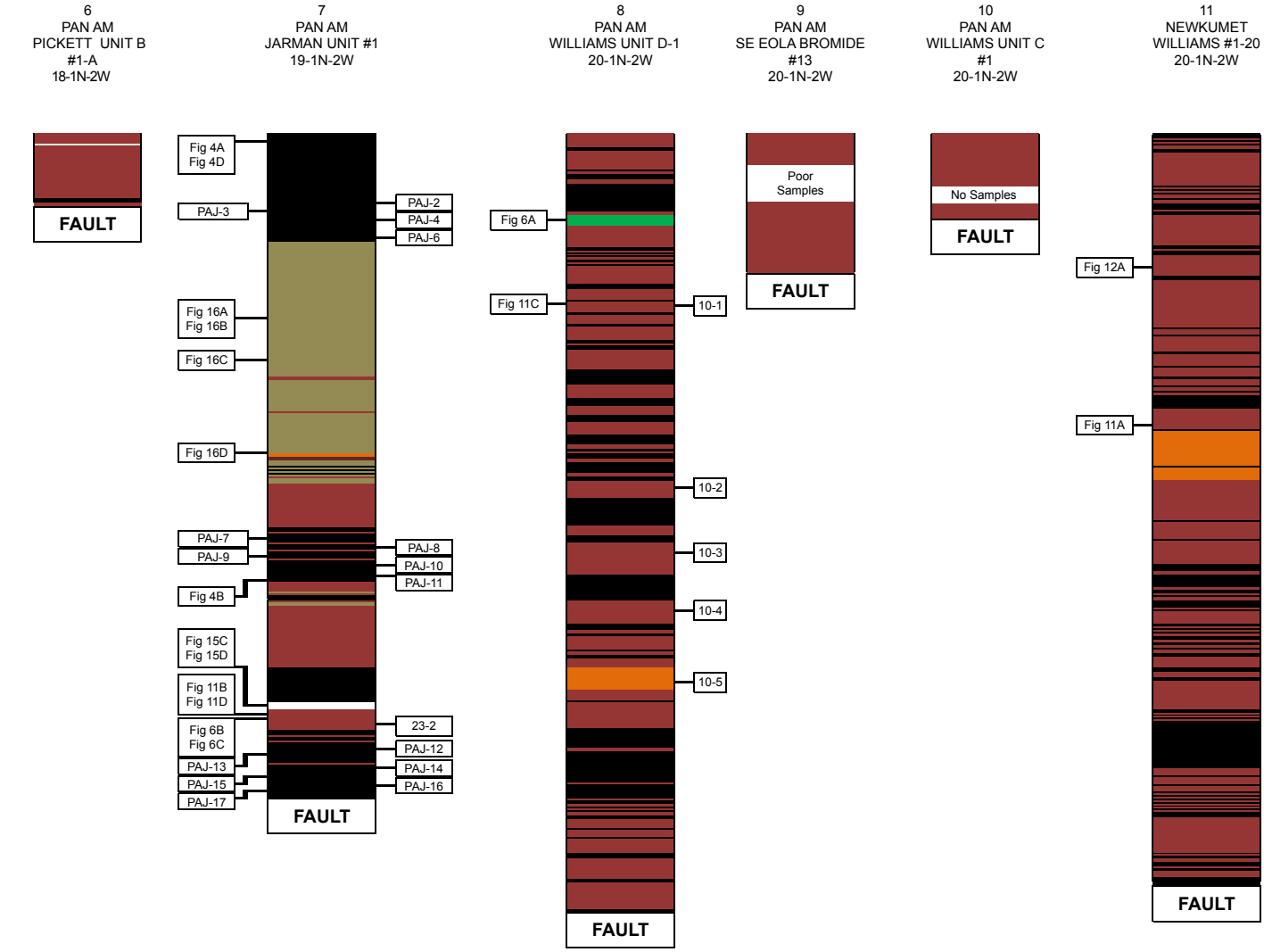


Legend

- Rhyolite
- Granite or Microgranite
- Basaltic to Intermediate Lavas or Diabase
- Mafic Phreatomagmatic Zone
- Terrigenous Clastic Sequence within Volcanic Section
- Rhyolitic Volcaniclastic Rocks
- Quartz Sandstone
- 12-3 — Felsic Geochemistry Sample Location
- PAN-14 — Mafic Geochemistry Sample Location
- Fig 4A — Photomicrograph Location
- GR-1 — Granite Thin Section Reference

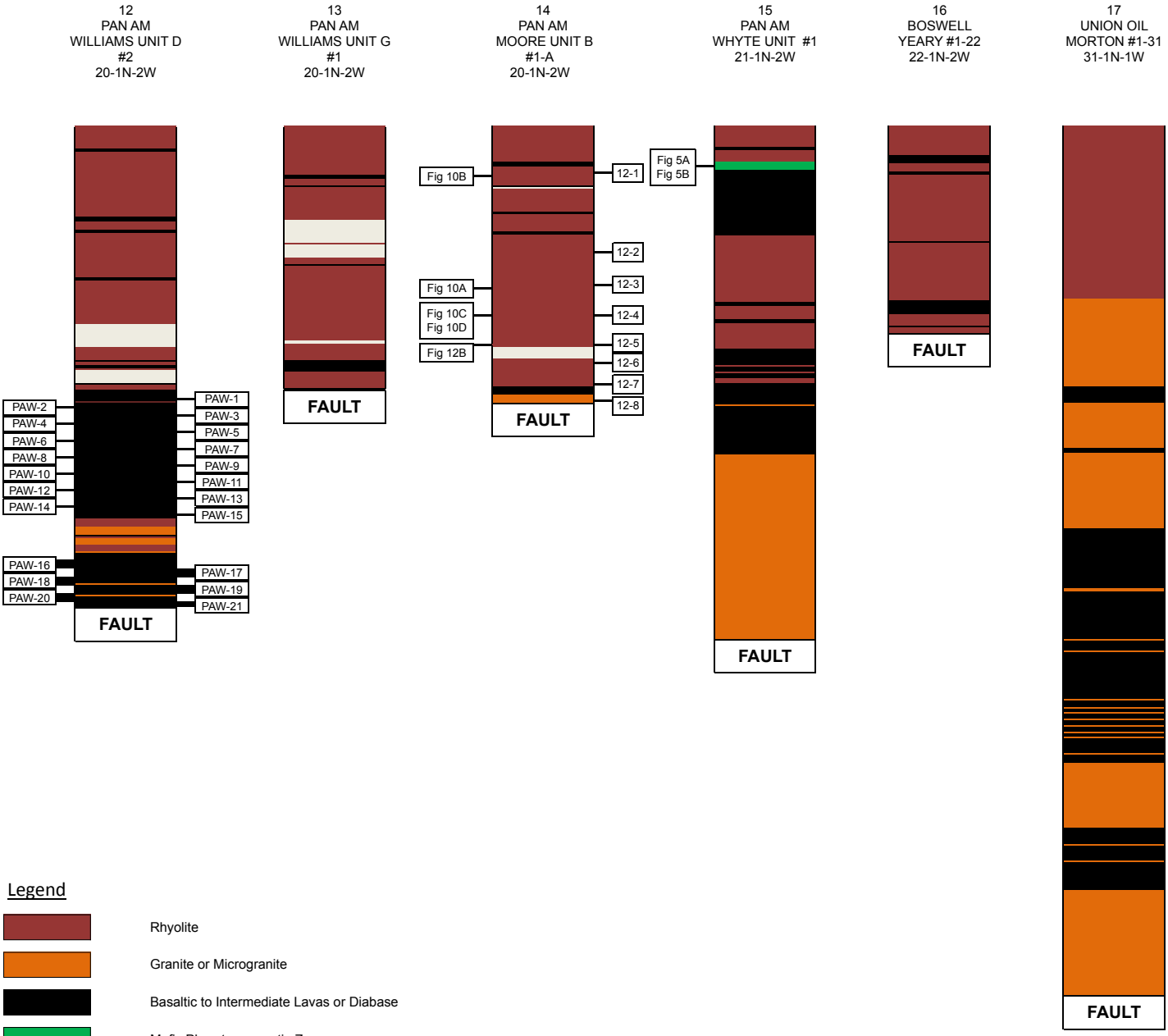


Legend

- Rhyolite
- Granite or Microgranite
- Basaltic to Intermediate Lavas or Diabase
- Mafic Phreatomagmatic Zone
- Terrigenous Clastic Sequence within Volcanic Section
- Rhyolitic Volcaniclastic Rocks
- Quartz Sandstone
- 12-3 — Felsic Geochemistry Sample Location
- PAN-14 — Mafic Geochemistry Sample Location
- Fig 4A — Photomicrograph Location
- GR-1 — Granite Thin Section Reference

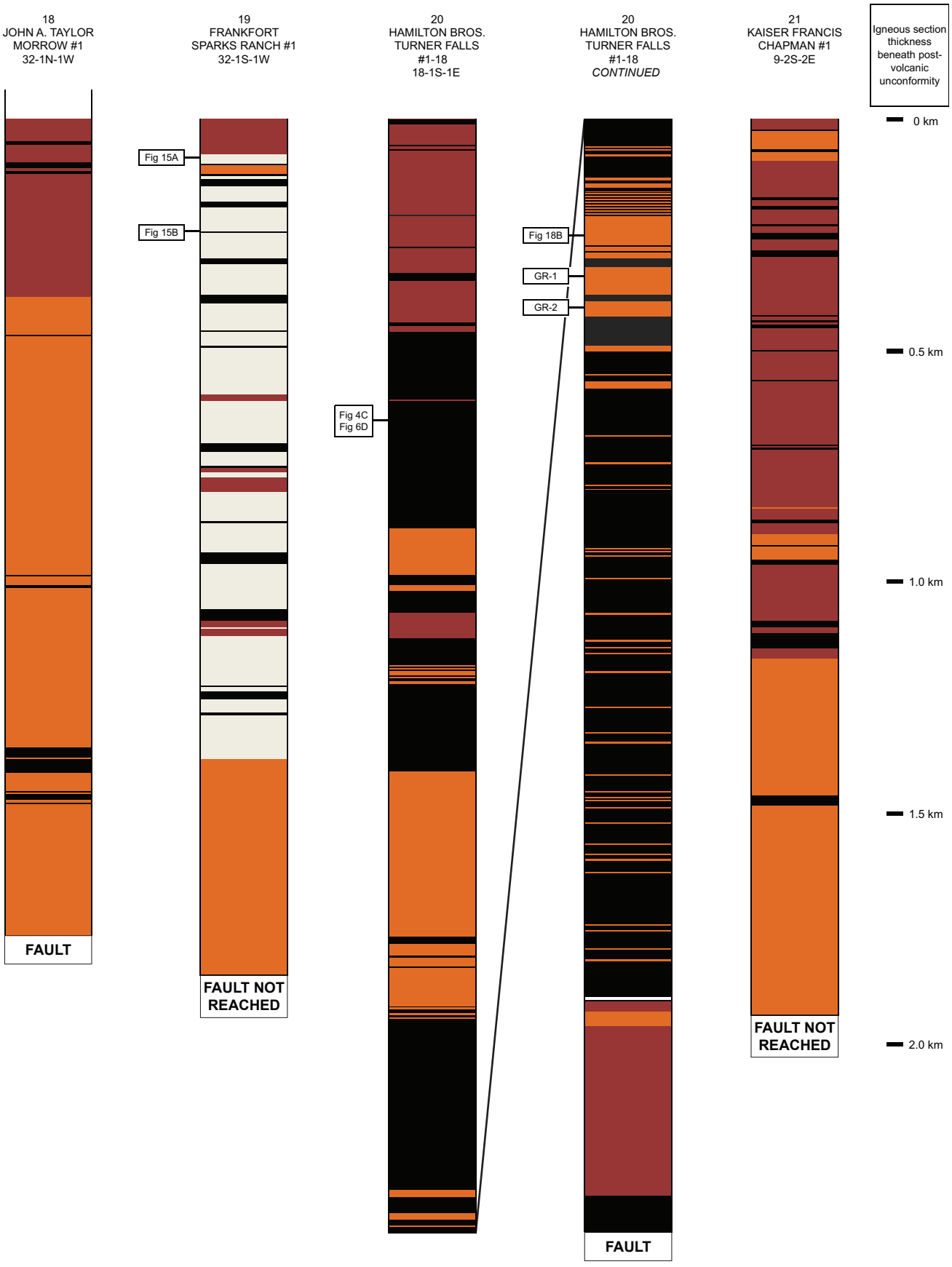
18
JOHN A. TAYLOR
MORROW #1
32-1N-1W
19
FRANKFORT
SPARKS RANCH #1
32-1S-1W
20
HAMILTON BROS.
TURNER FALLS
#1-18
18-1S-1E
20
HAMILTON BROS.
TURNER FALLS
#1-18
CONTINUED
21
KAISER FRANCIS
CHAPMAN #1
9-2S-2E
Igneous section thickness beneath post-volcanic unconformity
0 km
0.5 km
1.0 km
1.5 km
2.0 km
Fig 15A
Fig 15B
Fig 4C
Fig 6D
Fig 18B
GR-1
GR-2
FAULT
FAULT NOT REACHED
FAULT NOT REACHED
FAULT

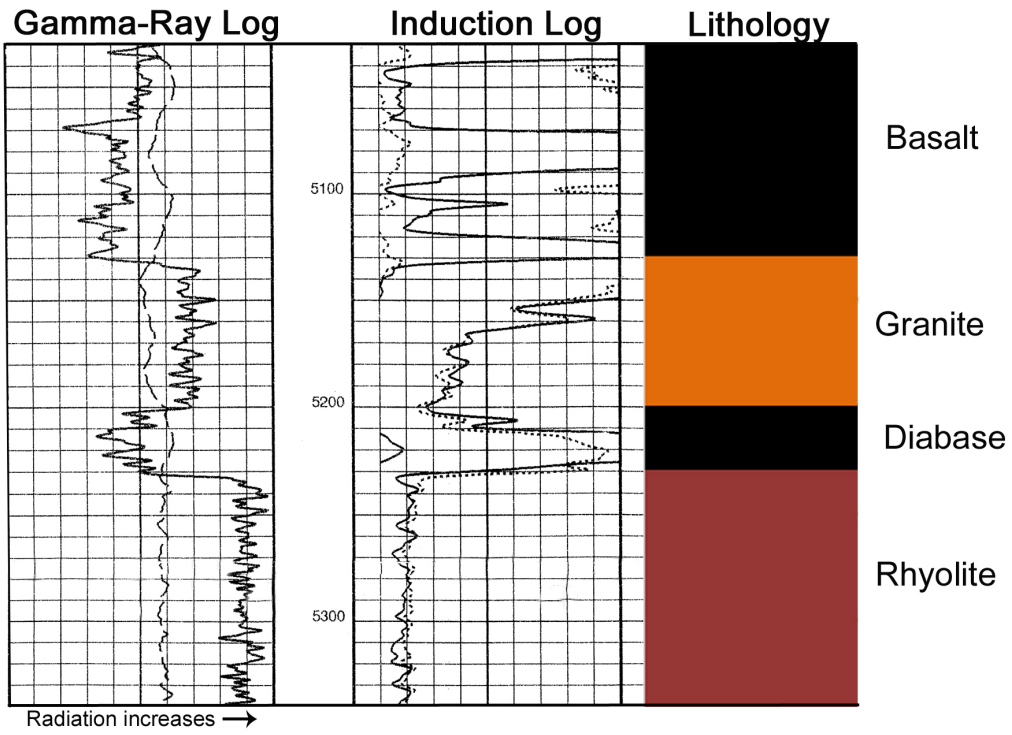


**Figure 3. Well-log interval from the COHO 4 Story showing GR and induction logs and corresponding lithologic log (depths are in feet). The GR log is very useful for determining lithology when paired with examination of drill cuttings.**

terval becomes apparent with increasing depth and penetration into the unweathered flow interior. Weathered rhyolite yields cuttings of a more neutral, typically brownish color with an indistinct matrix crystallinity and obscuration of the rhyolite texture by weathering products such as clays and oxides.

Flow boundaries may also be indicated by the presence of distinctive, originally glassy upper and lower flow margins (now altered and devitrified). Cuttings from these intervals are cryptocrystalline and typically dark-colored, and feldspar phenocrysts, when present, stand out clearly from the groundmass. The cuttings from these intervals tend to be equant in shape, whereas flow-interior rhyolite tends to break into "platy" cuttings with length and width dimensions four to six times their thickness. The devitrified glassy flow margins are similar to those documented from outcrop mapping of rhyolite cooling units in the Wichita and Arbuckle Mountains (see papers on the Carlton Rhyolite in this guidebook). Rhyolite cooling units in outcrop and in the subsurface are also identified by the presence of tridymite needles (inverted to quartz), which become visible in thin section inward from the chilled margins and which increase in size and frequency toward the center of the flow.

## BASALT AND DIABASE

Surface exposures of basalt in southern Oklahoma are limited to dikes thought to be part of a large dike swarm related to rifting (Denison, 1995). Until the examination of the Arbuckle wells, the only known eruptive basalts were found in eleven wells scattered over five counties in southwest Oklahoma, with the thickest drilled interval being 320 m. Ham et al. (1964) termed these rocks the Navajoe-Mountain Basalt Spilite Group. They considered this unit to be stratigraphically below the Carlton Rhyolite Group and inferred that parts of it were eroded prior to eruption of the rhyolites. In one well (the Stanolind 1 Perdasofpy), rhyolite overlies the basalt but is separated from it by a 183-m-thick granite sill. None of the western wells penetrated through the entire thickness of the basalts, leading to an uncertain placement of these rocks relative to the rhyolites.

In the Arbuckle area, the Hamilton Brothers 1-18A Turner Falls well drilled 4.8 km of rhyolite, granite, diabase, and basalt (Fig. 2). The borehole crossed the Washita Valley Fault at 4.8 km and proceeded to drill underthrust Ordovician dolomite to a total depth of 5.63 km. To the best of our knowledge, based on publicly available information, this is one of the thickest penetrations of igneous rocks in North America. The dominant lithology in this well is basalt, totaling over 2800 m. The basalt is intruded by diabase and multiple granites and is overlain by 530 m of rhyolite. A thin rhyolite layer interpreted to be intrusive occurs 164 m below the top of the basalt, and a 54-m-thick section of extrusive rhyolites is present 608 m below the top of the basalt. As discussed above, these values are apparent thicknesses.

### Basalt Petrography

As discussed below and in Brueseke et al. (this guidebook), geochemical analyses show that significant amounts of andesite are present with basalt in the three wells for

which such data are available. Because variably altered basalt and andesite cuttings are not readily distinguished under the binocular microscope or in thin section, we refer to all these rocks as basalt for the sake of convenience in the descriptions that follow. Plagioclase is the dominant phenocryst and is typically partly altered to sericite, epidote, prehnite, and/or carbonate. Mafic silicate phenocrysts also occur but are generally completely replaced by yellow-green to green clay (Fig. 4A). Based on the shapes of the pseudomorphs, olivine and pyroxene were originally present, and some relict clinopyroxene is still preserved. Vesicles are generally absent, but minor amounts of spherical or elongate, flow-aligned amygdules as much as 1.5 mm long occur in some cuttings and are filled with zeolites, green clay, or combinations of actinolite, green clay, quartz, and carbonate.

Replacement of the ferromagnesian minerals in some cases imparts a greenish hue to the cuttings, the depth of color indicating the degree of alteration. Carbonate alteration is indicated by anomalous medium- to light-gray colors in the cuttings, some of which show substantial replacement of plagioclase by carbonate minerals. Low-temperature hydrothermal activity characteristic of terrestrial volcanic fields and occurring during or shortly after accumulation of the volcanic pile, as well as deep brine migration from the adjacent 9-km-deep Ardmore Basin in the late Paleozoic, are thought to be responsible for the observed alteration patterns.

The basalts exhibit a wide range of groundmass textures, which can be distinguished in thin sections of all but the most altered samples. Intergranular texture consisting of randomly oriented plagioclase microlites with interstitial clinopyroxene, Fe-Ti oxides, and possibly altered olivine is common (Fig. 4B). Intersertal texture, in which the interstices between randomly oriented plagioclase microlites are filled with altered glass, is also present. In a smaller number of cuttings, tachylite makes up a major part of the groundmass and shows the dark, turgid appearance characteristic of this kind of basalt glass (Fig. 4C). The dark color is caused by a high content of mafic crystallites (e.g., Shelley, 1993), and the original glassy mesostasis between the crystallites has been altered to cryptocrystalline phases irresolvable at the highest magnification. Overall, the range of textures is typical of subaerial basalt lavas and reflects variable cooling rates depending on position within the flows. Intergranular textures formed during slower cooling in flow interiors, whereas intersertal and tachylitic textures indicate progressively more rapid cooling rates along the margins of flows (Williams et al., 1982; McPhie et al., 1993; Shelley, 1993).

It is impossible to determine the form and dimensions of the lava flows based on the limited data at hand. They may represent relatively small-volume flows supplied from fissures or central vents at various points in the rift. Flood basalts might also be present, although so far it has only been possible using geochemical criteria to correlate individual flows or groups of flows for relatively short distances between wells (Bulen, 2012; Brueseke et al., this guidebook).

The first basalts penetrated in the Pan Am 1-19 Jarman well at a depth of 945 m to 1020 m show a markedly different type of groundmass than the basalts described in the last paragraph. In all the thin sections from this interval the groundmass is dominated by variolitic texture, defined by radiating to plumose intergrowths of very fine grained, fibrous plagioclase and altered clinopyroxene (Figs. 4A and 4D). Somewhat coarser plagioclase microlites dispersed in the groundmass show distinctive swallow-tailed habits (Fig. 4D; Bryan, 1972). These textures typically develop in significant amounts where basalt lava is quenched by contact with water, resulting in rapid growth of groundmass phases under disequilibrium conditions (Bryan, 1972; Shelley, 1993). Aqueous quenching may have occurred where lava was erupted into lakes or where subaerial lavas encountered lakes as they flowed across the surface. Pillows might have formed in such cases but would be difficult to recognize based only on examination of cuttings. Swallow-tailed plagioclase microlites are also abundant in basalt at a depth of 1875 m in the Pan Am 1 Newberry well, although in this case they are enclosed within a matrix of altered glass, and variolitic texture is lacking. It is likely that the basalt in this interval also interacted with external water.

At a depth 1445 m to 1460 m in the Pan Am 1 Whyte well, basalt cuttings showing well-preserved pyroclastic textures are abundant (Fig. 5). This interval is overlain by rhyolite and rests on a thick interval of basalt. It has an irregular GR signature intermediate between these two rock types, indicating the presence of alternating basaltic and rhyolitic layers <3 m thick. We infer that several basaltic pyroclastic beds were penetrated in this interval. The intercalated rhyolite units are too thin to be normal rhyolite flows and are probably volcaniclastic deposits. Similar basaltic pyroclastic cuttings to those present in the Pan Am 1 Whyte well occur at a depth of 1200 m in the Pan Am D-1 Williams well (Fig. 6A) and at 1950 m in the Pan Am 1-19 Jarman well (Figs. 6B and 6C). In both these cases the basaltic pyroclastic cuttings occur with more abundant rhyolite cuttings and are inferred to come from thin basaltic pyroclastic intervals intercalated with the rhyolites.

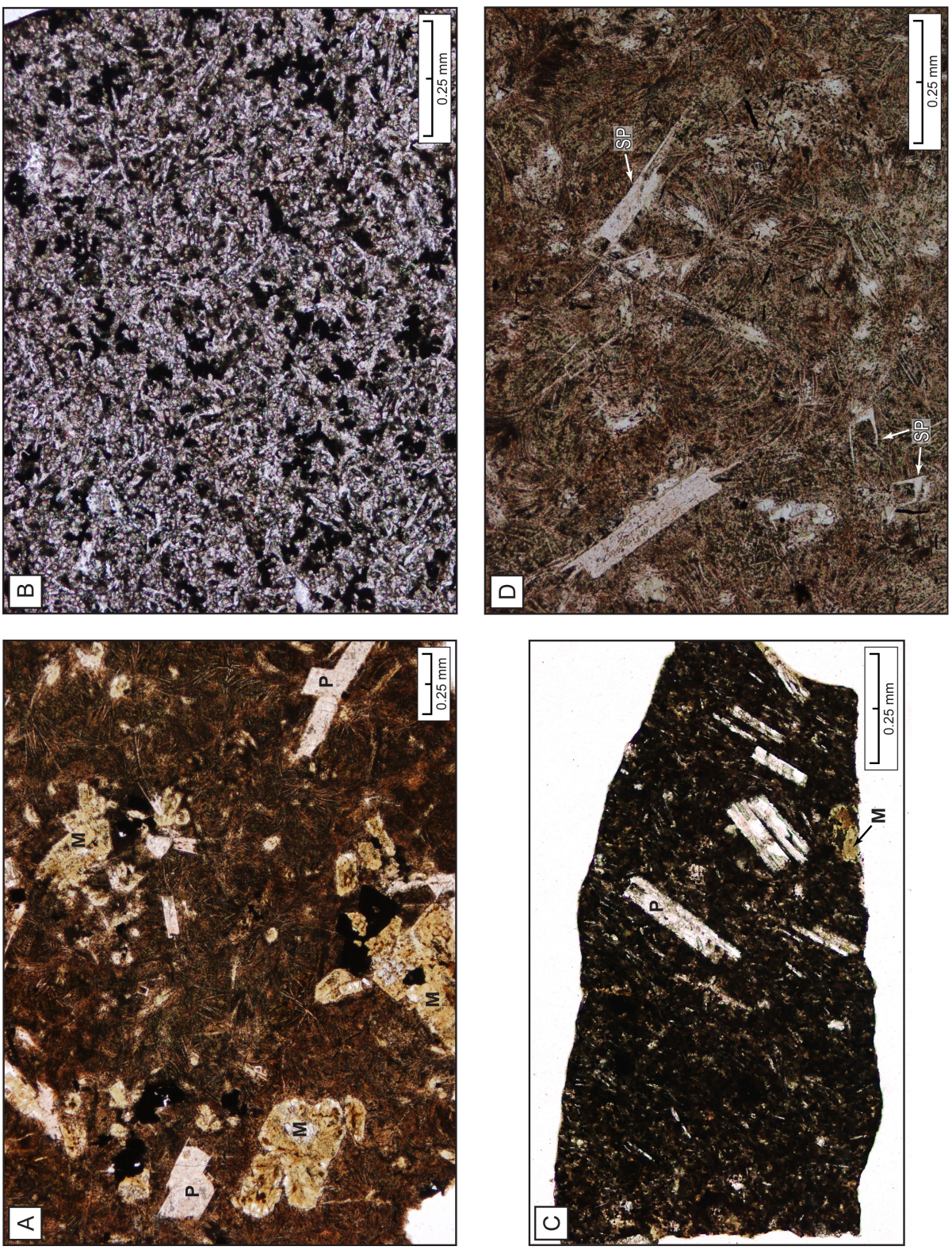


**Figure 4. Photomicrographs of basalt cuttings, all in plane light; locations in wells are shown in Figure 2. (A) Pan Am 1-19 Jarman. Phenocrysts of plagioclase (*P*) and mafic silicates (*M*) replaced by yellow-green clay. Dark groundmass shows variolitic texture. (B) Pan Am 1-19 Jarman. Randomly oriented plagioclase microlites within typical intergranular groundmass; interstices between plagioclase microlites are occupied by mafic silicates and opaque Fe-Ti oxides. (C) Hamilton Brothers 1-18A Turner Falls. Flow-aligned plagioclase microlites (*P*) set in a tachylitic groundmass; *M*: mafic silicate replaced by green and brown clay. (D) Pan Am 1-19 Jarman. Variolitic texture and swallow-tailed plagioclase microlites (*SP*).**

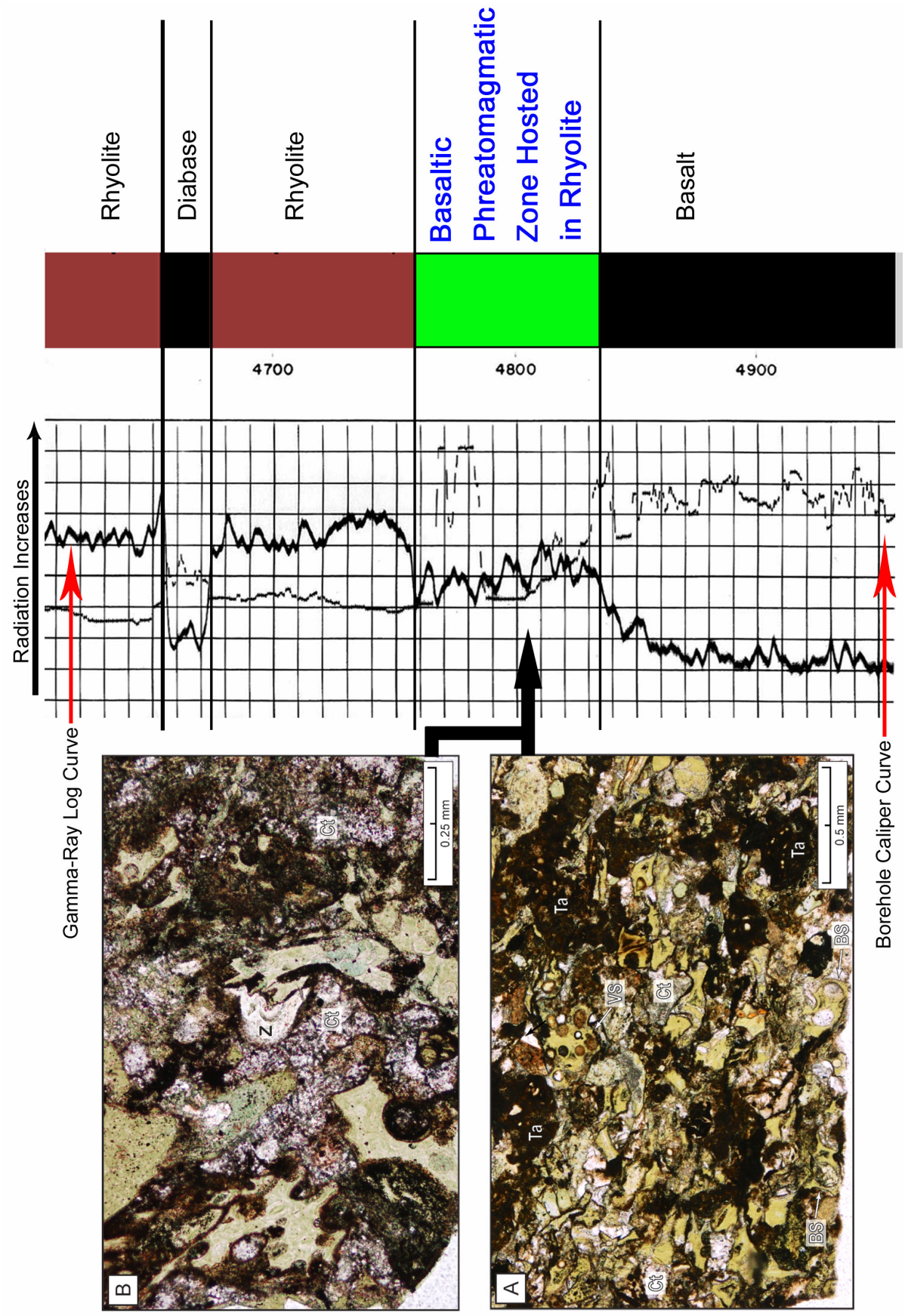


**Figure 5. Phreatomagmatic section from the Pan Am 1 Whyte illustrating basaltic phreatomagmatic deposits hosted in rhyolite; depth is indicated in feet. GR log records low gamma-ray values for basalts and diabases and higher values for granites and rhyolites; complex mixing of lithologies in the phreatomagmatic section produces intermediate values. Photomicrographs (in plane light) show basaltic phreatomagmatic ash shards consisting mostly of sideromelane replaced by green clay; gray or clear areas between pyroclasts consist of zeolite (*Z*) and carbonate (*Ct*) cement. (A) Sideromelane shards intermixed with lesser amounts of dark tachylite clasts (*Ta*); *VS*: example of vesicular shard; vesicles are filled with brown clay, carbonate, and zeolites; *BS*: examples of bubble-wall shards. (B) Closer view of sideromelane shards with margins partly defined by broken bubble walls.**

In the cuttings from all three wells (Pan Am 1 Whyte, D-1 Williams, and 1-19 Jarman), some of the ash- and lapilli-size basaltic pyroclasts are relatively unaltered tachylite, but most were originally composed of transparent glass that has now been replaced by green clay, yellow-brown to orange- or red-brown palagonite, and/or zeolites (Figs. 5A and 5B; 6A, 6B, and 6C). Such an alteration assemblage is diagnostic of original sideromelane, and the characteristic light-brown color of this type of basalt glass is preserved to a certain extent in some samples (Fig. 6A). Sideromelane is produced when basalt magma is chilled so rapidly by contact with external water that groundmass phases have little or no time to nucleate and grow, forming an essentially pure glass. This type of glass is particularly unstable and highly susceptible to alteration, as seen in the present case.

Zeolites and/or carbonates occur as cement between the ash and lapilli particles (Figs. 5A and B; 6A, 6B, and 6C), and cementation probably occurred early in the diagenetic history, so that delicate pyroclast morphologies were protected from significant compaction during burial. The coarser pyroclasts have variable amounts of vesicles filled with green clay and/or zeolites, and some have fluidal outlines (Fig. 6B). Some finer grained pyroclasts are bubble-wall shards (Fig. 6A), but the margins of many pyroclasts are controlled by planar or curviplanar fractures rather than broken bubble walls (Figs. 5A and 5B; 6A). Pyroclast shapes and the abundance of sideromelane are diagnostic of violent phreatomagmatic disruption of basalt magma driven by gases exsolving from the magma combined with steam explosivity generated by rapid heating of external water. Tachylite pyroclasts mixed with the sideromelane particles (Fig. 5A) were most likely derived from less rapidly quenched batches of magma [see Eschberger and Hanson paper (this guidebook) for further discussion and relevant references]. Such phreatomagmatic eruptions could have occurred where basalt magma interacted explosively with lake water or encountered groundwater-rich horizons during its ascent, generating phreatomagmatic explosions of the type seen in many subaerial basalt provinces (White and Ross, 2011). We became aware of the existence of basalt cuttings showing pyroclastic textures relatively late in our study of the wells described herein, and it is likely that further examination of cuttings from these wells will reveal additional examples.

## Diabase

Ham et al. (1964, p. 78) reported that across all the subsurface igneous sections examined in their study, "The number of wells in which diabase has been found is unexpectedly large." In our study, diabase occurs in all but two wells (the two wells with the shortest penetration of igneous section). Diabase occurs as intrusions in all rock types below the Upper Cambrian unconformity in thicknesses ranging to as much as 35 m but more typically between 3 m and 10 m. Diabase is an important, although minor, constituent of the exceptionally thick mafic section in the Hamilton Brothers 1-18A Turner Falls well. The diabase intrusions are probably for the most part sills or subhorizontal sheets, because intersecting a subvertical dike in a borehole would require a fortuitous set of circumstances.

Many examples occur where cuttings indicate the presence of several thin diabase sheets intrusive into 50-m- to 80-m-thick rhyolite or granite intervals, although the individual diabase intrusions are too thin to be discernible on GR logs. Diabase is typically found intruded into zones of weakness such as rhyolite flow boundaries or volcaniclastic beds. Thermal alteration of rhyolites occurs adjacent to diabase intrusions, especially where multiple, closely spaced intrusions are present. Thermally altered rhyolite is identified in drill cuttings by a color change to more neutral gray or tan and a "grainy" appearance due to recrystallization of the constituent minerals. More highly altered samples typically have a milky neutral gray color and a uniform texture.

### Diabase Petrography

The diabases show a range in grain size reflecting different cooling rates. In the coarsest samples, which presumably come from the interiors of thicker intrusions, plagioclase and clinopyroxene crystals are ≥2 mm long and show ophitic texture. In some cases these minerals are only slightly altered (Fig. 6D). Pseudomorphs of green and brown clay after olivine occur next to nearly pristine clinopyroxene even in the freshest samples (Fig. 6D). Other primary igneous phases include biotite, Fe-Ti oxides, and apatite.

Many of the diabases are highly altered. Plagioclase alteration products are similar to those in the basalts and include sericite, epidote, prehnite and/or carbonate. Actinolite, epidote, titanite, and green to brown clay are the principal alteration products of clinopyroxene, which in the more altered samples is either completely replaced or survives as small relics engulfed within intergrowths of the secondary phases. A few of the more highly altered diabases show cataclastic textures in thin section, suggesting that some of the alteration resulted from ingress of hydrothermal fluids along fault zones.

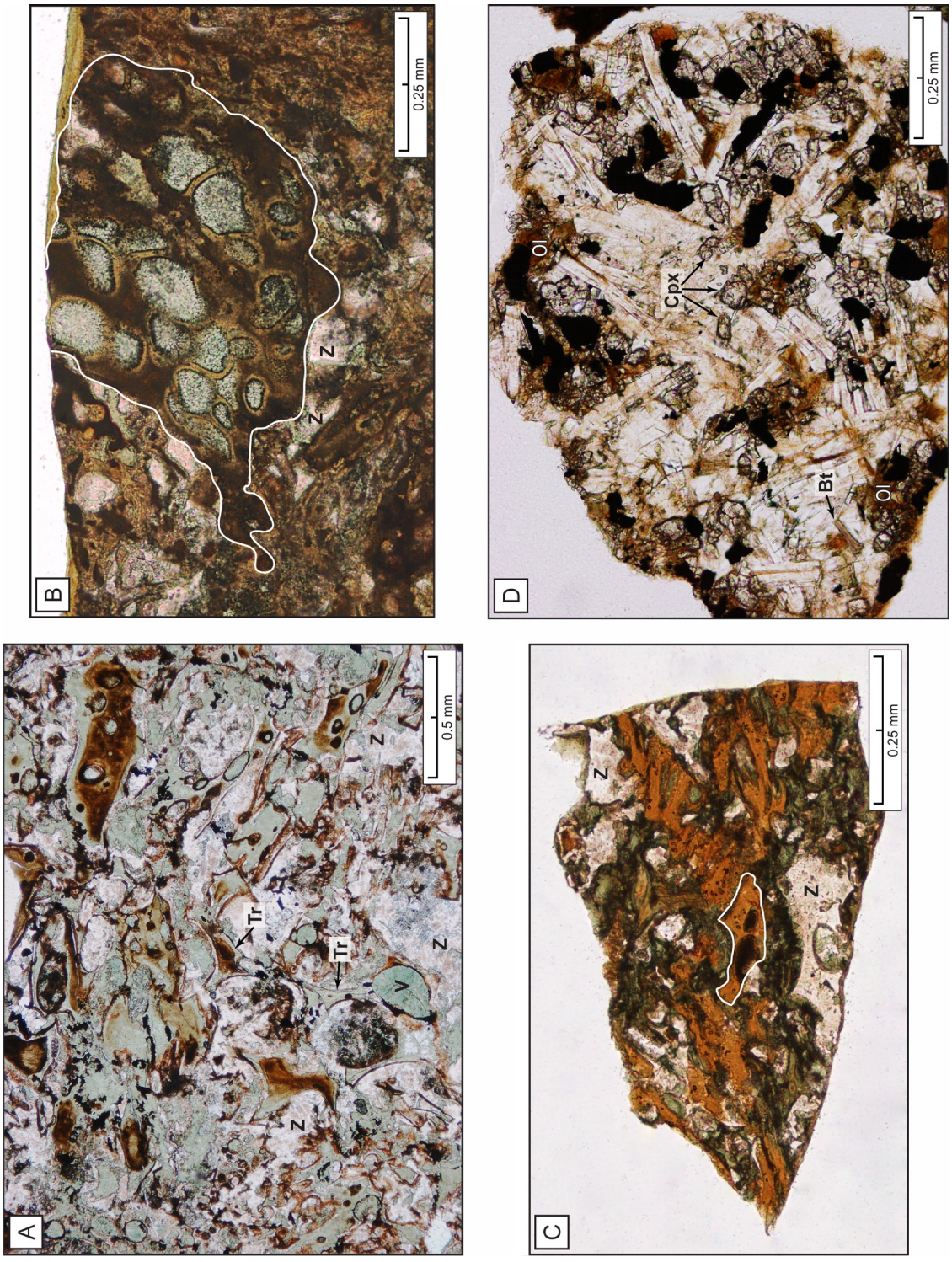


**Figure 6. Photomicrographs of basaltic pyroclastic rocks and diabase, all in plane light; locations in wells are shown in Figure 2; gray or clear areas between pyroclasts in figures A, B, and C consist primarily of zeolite cement (*Z*). (A) Pan Am D-1 Williams. Sideromelane shards partly replaced by green clay; remnants of original brown sideromelane are preserved in some shards but are altered to a cryptocrystalline intergrowth of secondary phases. *Tr*: tricuspate bubble-wall shards; *V*: vesicle filled with green clay. (B) Pan Am 1-19 Jarman. Fluidal, moderately vesicular pyroclast of altered sideromelane with margin outlined in white; vesicles are filled with green clay and zeolites. (C) Pan Am 1-19 Jarman. Small ash shards consisting of sideromelane replaced by orange-brown palagonite; margin of one shard is outlined. (D) Hamilton Brothers 1-18A Turner Falls. Relatively fresh diabase. Plagioclase crystals are clear, magnetite is opaque; *Cpx*: clinopyroxene; *Ol*: olivine replaced by brown clay; *Bt*: biotite.**

## Geochemistry of Basaltic Intervals

Major- and trace-element analyses of broadly mafic well cuttings from the Pan Am 1 Newberry, Pan Am D-2 Williams, and Pan Am 1-19 Jarman wells were obtained using x-ray fluorescence spectroscopy (Brueseke et al., this guidebook). The analyzed cuttings generally have a basaltic or diabasic appearance under a binocular microscope, and this is confirmed by thin-section study of a few representative intervals. Forty-eight samples were analyzed and range in composition from basalt to andesite (volatile-free) (Fig. 7A), and follow a subalkaline differentiation array. Data from subsurface felsic samples discussed later in this paper are also shown in Figure 7A. The igneous suite is bimodal — there is a distinct compositional gap between the andesites and the felsic rocks. The mafic and intermediate rocks are primarily tholeiitic (Fig. 7B), as are the diabase intrusions and gabbros elsewhere in the Wichita Province. Silica values range from 47.58 to 61.76 wt %, and on Harker diagrams low- and high-silica samples define arrays consistent with fractional crystallization (likely coupled with upper crustal contamination) of a "typical" mafic assemblage dominated by olivine and plagioclase feldspar (e.g., increasing incompatible element abundance with silica increase; Bulen, 2012; Brueseke et al., this guidebook). Bulen (2012) and Brueseke et al. (this guidebook) demonstrate that the incompatible trace-element geochemistry of these cuttings is consistent with an enriched mantle source (e.g., OIB-source enriched mantle).

Many of the thicker basalt intervals likely represent distinct "groups." Based on his study of the Pan Am 1 Newberry, D-2 Williams, and 1-19 Jarman wells (Fig. 8), Bulen (2012) suggested that the distinct compositional groups are reflected in geochemical variations in the extrusive basalt pile. The differences in Ni content (Fig. 8) are mirrored by differences in other major and trace elements (e.g., $SiO_2$, FeO*, Zr, etc.) and incompatible trace-element ratios (e.g., K/P, etc.). Bulen (2012) interpreted these data to reflect the occurrence of stratigraphically and temporally distinct groups of lavas, each group sourced from a distinct magmatic system. Similar relationships are found in drill core of Pleistocene to Pliocene basalts from the Snake River Plain, Idaho (Hughes et al., 2002; Shervais et al., 2006; Jean et al., 2013). Furthermore, it is possible that the variations in the Pan Am D-2 Williams well (Fig. 8; distinct Ni compositional differences where low-Ni samples have high Zr, $SiO_2$, and K/P and less evolved high-Ni samples have low Zr, $SiO_2$, and K/P; Bulen, 2012) reflect a similar situation to that outlined by Shervais et al. (2006) and Jean et al. (2011) for the Snake River Plain where the chemical/isotopic changes exhibited by subsurface flow groups reflect temporally distinct recharge and fractionation ± assimilation cycles of mafic magma sourced from a layered mafic intrusive complex in the middle crust.

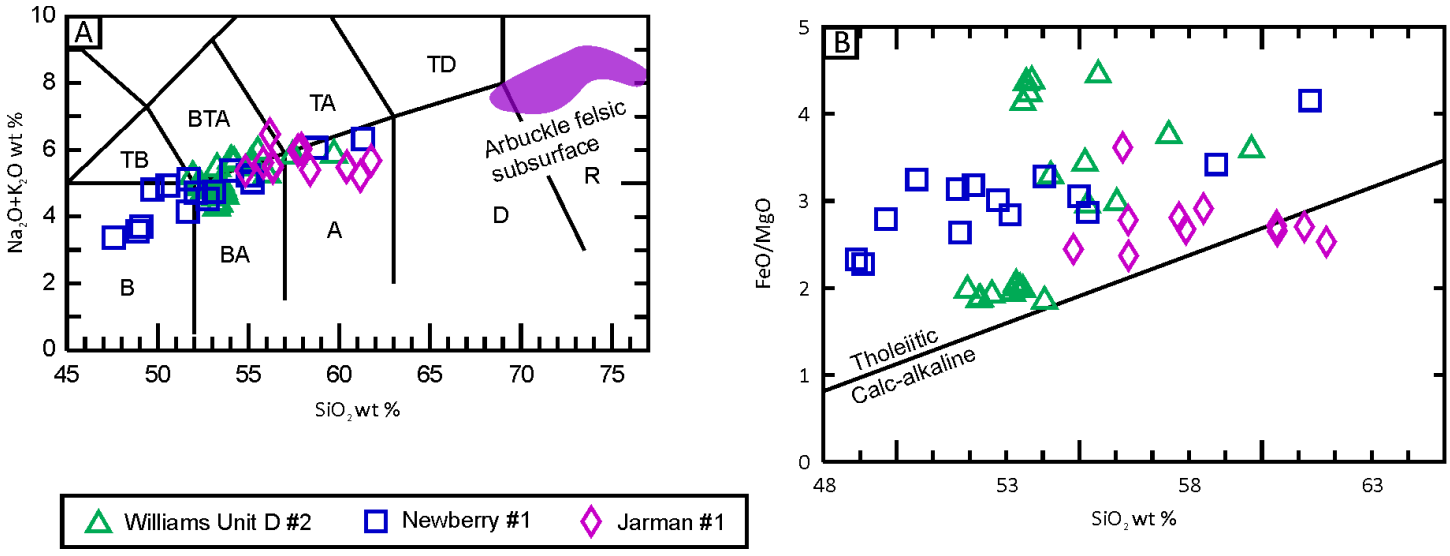


**Figure 7. (A) Igneous rock classification based on total alkalis vs. silica (Le Bas et al., 1986). Arbuckle felsic subsurface field includes rhyolite lavas and two granite samples as discussed in this paper. B: basalt; TB: trachybasalt; BA: basaltic andesite; BTA: basaltic trachyandesite; TA: trachyandesite; A: andesite; TD: trachydacite; D: dacite; R: rhyolite. (B) Tholeiitic vs. calc-alkaline discrimination diagram of Miyashiro (1974).**

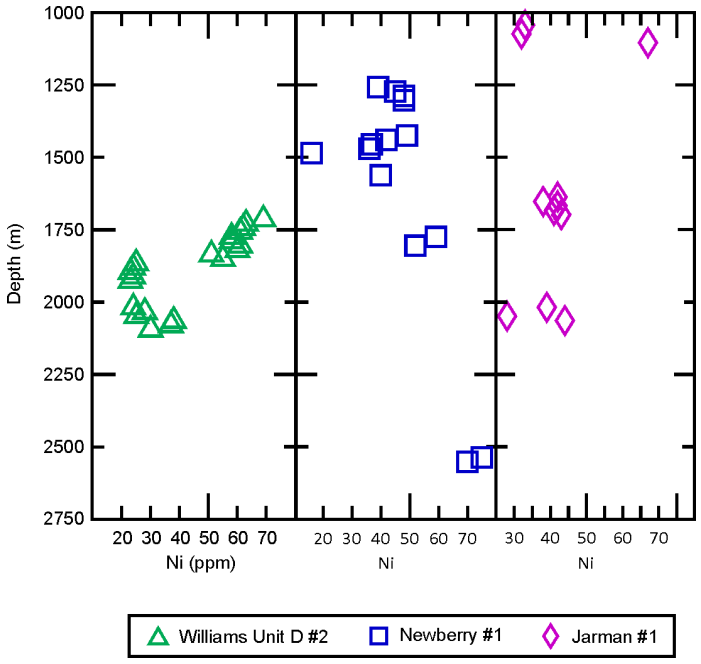


**Figure 8. Ni concentrations (ppm) as a function of depth of samples from the three wells studied by Bulen (2012).**

## RHYOLITE

There is no evidence for explosive caldera-type rhyolitic volcanism in southern Oklahoma. Effusive rhyolite lavas are interpreted to have erupted from linear vents (Hanson et al., 2013). Some of the subsurface rhyolite flows documented in the present study are more than 400 m thick, in agreement with results from surface mapping. The generalized rhyolite cooling unit developed from surface mapping (Hanson et al., 2013; Hanson et al., this guidebook) and based partly on occurrence and dimensions of tridymite needles can also be applied to the subsurface. Figure 9 shows a subsurface cooling unit in the Pan Am 1-A Moore well. The upper flow boundary is defined by a chilled interval interpreted to be the base of an overlying flow, with a diabase sill intruded at the flow boundary. The lower boundary is defined by abrupt textural changes. Thin sections show that the length and abundance of tridymite needles (inverted to quartz) increase towards the middle of the flow.

### Rhyolite Petrography

Examination of cuttings under the binocular microscope suggests that the rhyolite intervals in the wells are lava flows and not pyroclastic rocks, and this has been confirmed by thin-section study. Reworked rhyolitic volcaniclastic rocks occur in some wells and are described below. Feldspars are the most common phenocrysts in the lavas and are predominantly plagioclase, although smaller amounts of alkali feldspar (probably relict sanidine) are also present (Fig. 10A). Phenocrysts of chessboard albite in some samples (Fig. 10B) indicate replacement of original alkali feldspar by Na-rich fluids. The feldspars are generally clouded by very fine grained, disseminated hematite (Fig. 10A), as is typical of feldspars in surface exposures of Carlton Rhyolite, and show relatively minor alteration to carbonate, sericite, or green clay. Mafic silicate phenocrysts occur in variable amounts and are completely replaced by green clay intergrown with fine-grained magnetite and leucoxene (Fig. 10A); the shapes of the pseudomorphs suggest they were originally pyroxene or possibly fayalite. Quartz phenocrysts have not been observed in the rhyolite lavas although monocrystalline quartz grains in some of the volcaniclastic intervals are inferred to represent phenocrysts liberated during erosion of rhyolites not penetrated by the studied wells.

Epidote, carbonate, and/or green clay locally replace parts of the groundmass, but the original textures are generally well preserved (except that all glass has devitrified). One notable difference between the subsurface rhyolites in the wells shown in Figure 2 and most of the exposed parts of the Carlton Rhyolite is that tridymite crystals are much less common in the groundmass of the subsurface examples studied so far in thin section and are only abundant in the Pan Am 1-A Moore well. In cuttings from that well the tridymite ranges in length from ≤0.03 mm to 0.5 mm (Figs. 9, 10C, and 10D), which is inferred to reflect variable cooling rates in relatively thick lavas, by analogy with outcrop studies of the rhyolites described in other papers in this volume.

In the other intervals of rhyolite penetrated by the wells, groundmass textures indicate significantly more rapid cooling, probably of thinner or more restricted lava flows. Delicate flow lamination of the type present in some Carlton Rhyolite outcrops is only rarely seen in the cuttings from these intervals, but irregular to ellipsoidal and elongate amygdules as much as 2 mm or more in length are common and are filled with quartz, chalcedony, and/or carbonate. Relict perlitic texture is widely developed and records hydration of glass (Fig. 11A). Spherulites are also common and either occur separately in the groundmass or form coalescing masses (Figs. 11B, 11C, and 11D); some spherulites extend outward from phenocryst margins, which served as nucleation sites. The largest spherulites observed are ~2 mm across and consist predominantly of fibrous, radially arranged alkali feldspar with interstices between

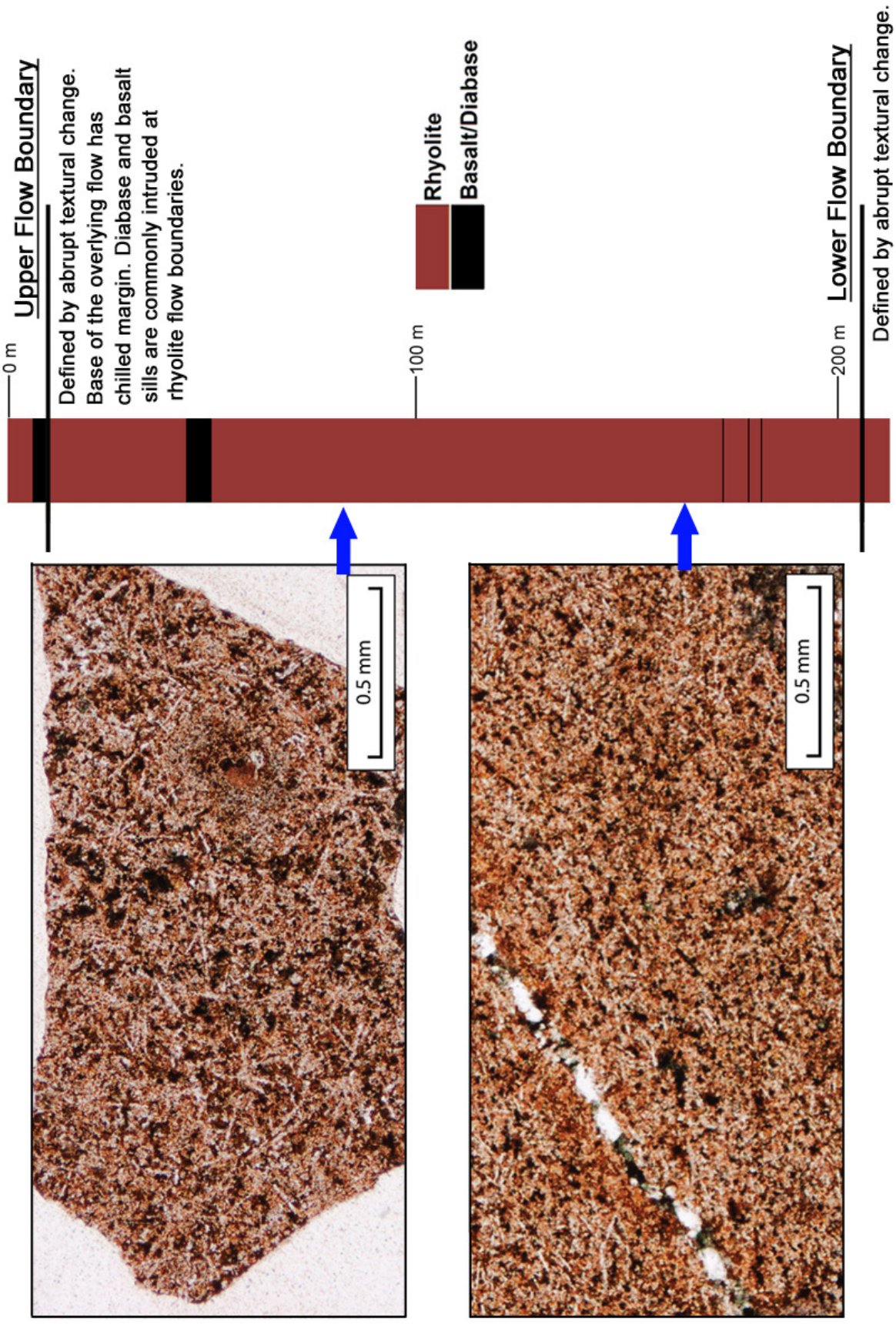


**Figure 9. Subsurface rhyolite cooling unit identified in the Pan Am 1-A Moore. Photomicrographs show increase in tridymite needle size and abundance toward the center of the flow. Tridymite has inverted to quartz.**

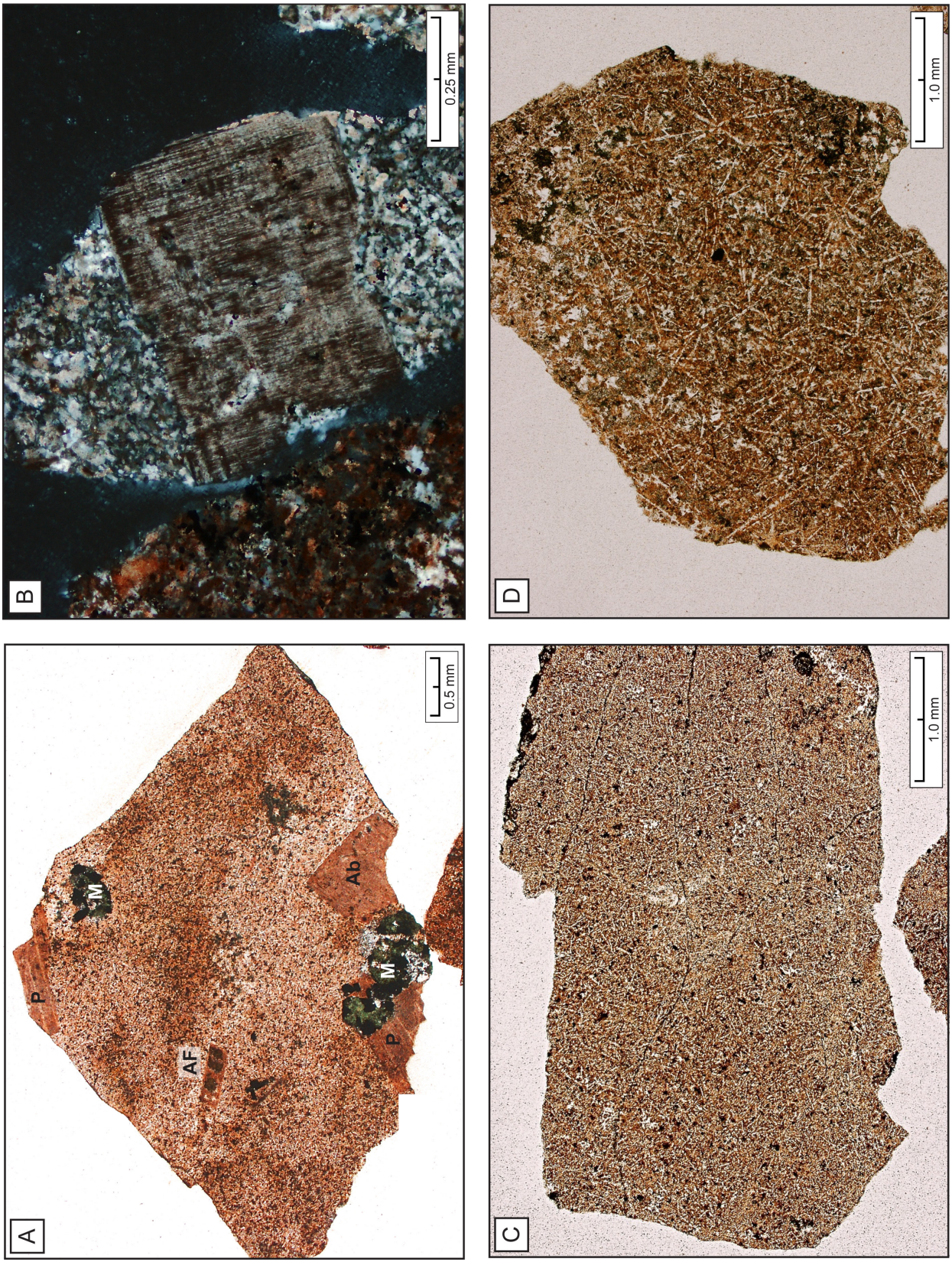


**Figure 10. Photomicrographs of rhyolite cuttings, all from the Pan Am 1-A Moore (Fig. 2); A, C, and D in plane light, B in crossed polars. (A) Rhyolite with groundmass containing tridymite needles (inverted to quartz). Phenocrysts consist of plagioclase (*P*), chessboard albite (*Ab*), alkali feldspar (*AF*), and mafic silicates (*M*); the latter are replaced by green clay, magnetite, and leucoxene. (B) Chessboard albite replacing alkali feldspar phenocryst; groundmass consists of microcrystalline intergrowth of quartz and feldspar. (C) Fine-grained tridymite crystals in groundmass. (D) Coarser tridymite in another cutting, taken at same scale as C.**

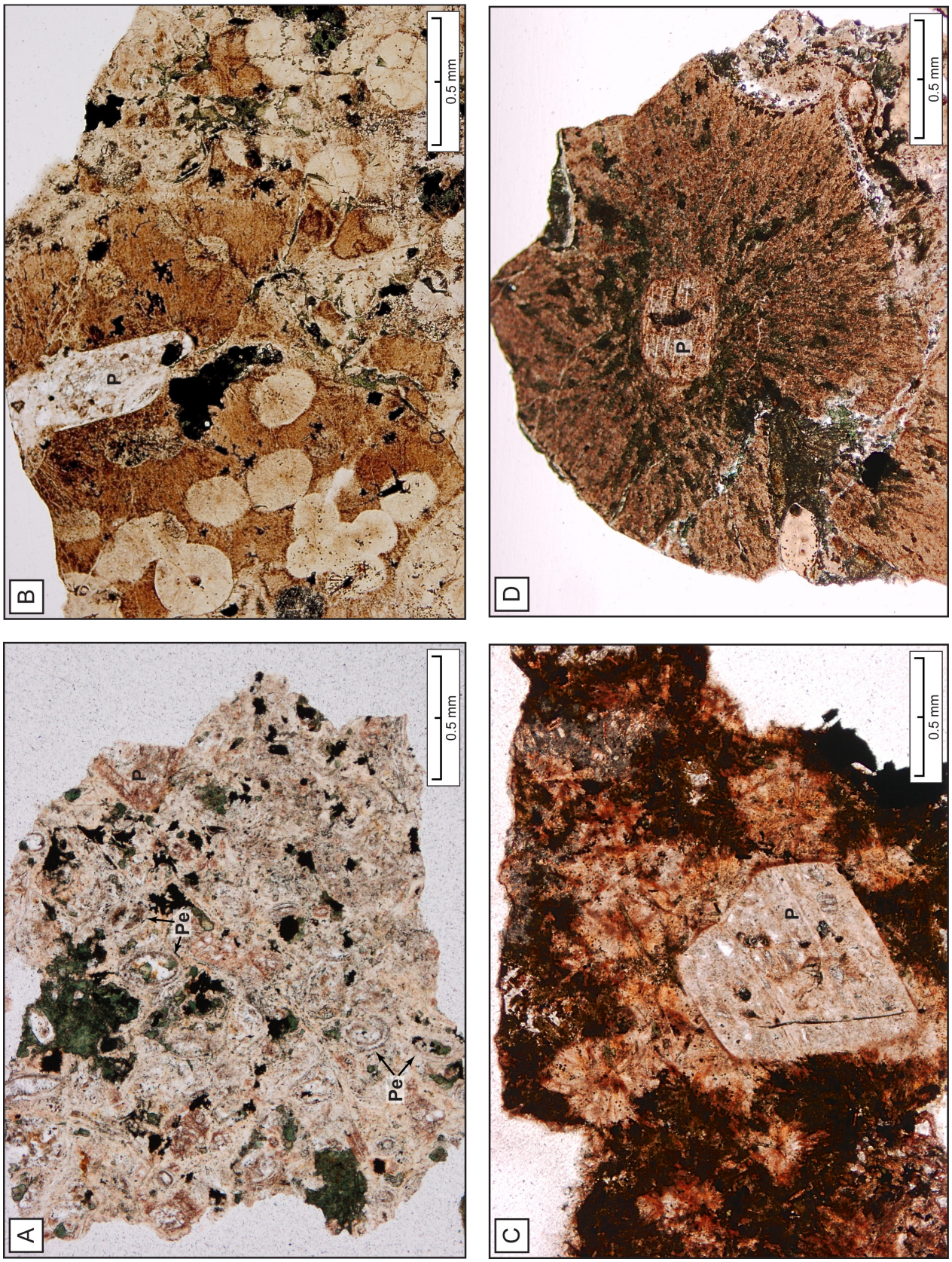


**Figure 11. Photomicrographs of perlitic and spherulitic textures in rhyolite cuttings, all in plane light; plagioclase phenocrysts (*P*) are visible in all four photos; locations in wells are shown in Figure 2. (A) Newkumet 1-20 Williams. Relict perlitic texture, with examples of curved cracks indicated (*Pe*). Note aggregates of green clay replacing groundmass in places. (B) Pan Am 1-19 Jarman. Small clear spherulites consisting of very fine grained, radiating crystal fibers. (C) Pan Am D-1 Williams. Coalescing spherulites, some of which have nucleated on plagioclase phenocryst. (D) Pan Am 1-19 Jarman. Coarser spherulite extending from plagioclase phenocryst.**

the feldspar fibers filled either with very fine grained quartz and/or granules or elongate crystals of magnetite (Fig. 11D). The spherulites range downward in diameter to ~0.03 mm, and the smaller examples consist of extremely thin crystal fibers that are too fine grained for rigorous identification (Fig. 11B). By analogy with experimental studies (Lofgren, 1971), the spherulites consisting of coarser crystals (fibers with larger diameters) presumably formed at higher temperatures than those consisting of finer fibers. Some of the coarser spherulites may have developed in undercooled melt above the glass transition temperature, as discussed in Hanson and Eschberger paper (this guidebook), but the majority probably formed during primary devitrification of glass as the flows cooled from magmatic temperatures. In many cases, spherulitic crystallization was preceded by growth of thin blades or elongate microlites of magnetite (now partly oxidized to hematite) that are either straight or curved (Fig. 12A) and represent an early stage of crystal nucleation and growth. Where spherulites are absent, the groundmass in some samples exhibits well-developed snowflake texture (Fig. 12B), which is another common feature that forms during primary devitrification of rhyolite glass. In other samples the groundmass consists of an intergrowth of roughly equidimensional, microcrystalline to cryptocrystalline quartz and feldspar that overprints flow lamination and perlitic texture and is inferred to have formed during slow devitrification of glass after the flows had cooled to ambient temperatures.

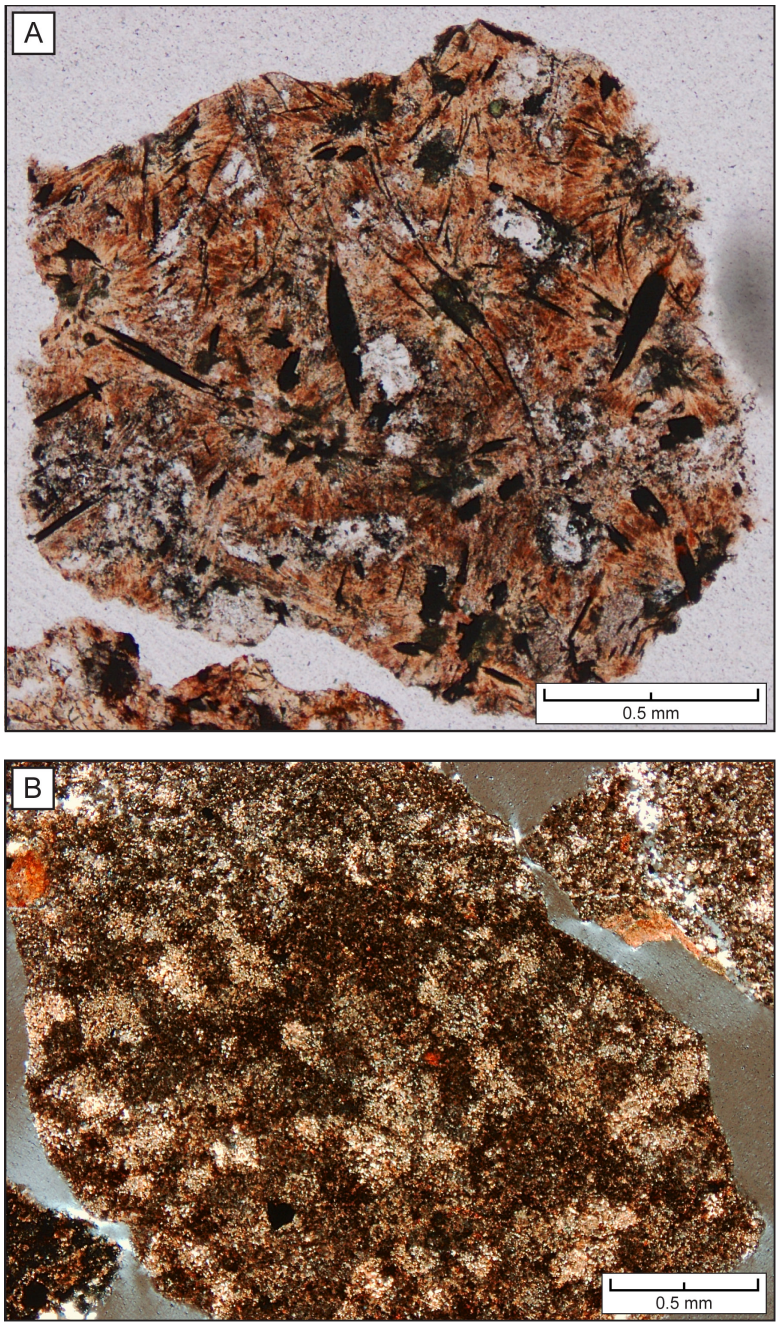


**Figure 12. Photomicrographs of groundmass textures in rhyolite cuttings, both in plane light; locations in wells are shown in Figure 2. (A) Newkumet 1-20 Williams. Thin blades and narrow, elongate crystals of magnetite (opaque), which predate crystallization of spherulites (orange-gray to brown shades). (B) Pan Am 1-A Moore. Snowflake texture, defined by micropoikilitic quartz enclosing numerous tiny feldspar microlites.**

**Rhyolite Geochemistry**

Geochemical analyses of seven representative rhyolite samples from the Pan Am 1-A Moore, four samples from the Pan Am D-1 Williams, one sample from the Pan Am 1-19 Jarman, and two samples from thin granite intervals are given in Table 2 (sample locations in the wells are shown in Figure 2). Major-element contents for the rhyolite samples overlap much of the compositional range shown by the Carlton Rhyolite as a whole (Hanson and Eschberger paper, this guidebook). Silica values for the subsurface samples range from 68.83 to 74.50 wt % (volatile-free), except for granite sample 12-8, which has a silica content of 76.64 wt %. On Harker diagrams (Fig. 13) the data tend to exhibit typical igneous trends, with $TiO_2$, FeO, MgO, CaO, and $P_2O_5$ showing overall decreases with increasing silica. Although evidence for significant

TABLE 2: GEOCHEMICAL DATA FOR SUBSURFACE RHYOLITE AND GRANITE SAMPLES

| | Pan Am D-1 Williams | | | | | Pan Am 1-A Moore | | | |
|---|---|---|---|---|---|---|---|---|---|
| | Rhyolite | | | | Granite | Rhyolite | | | |
| **Normalized major elements (wt %)*** | | | | | | | | | |
| **Sample:** | **10-1** | **10-2** | **10-3** | **10-4** | **10-5** | **12-1** | **12-2** | **12-3** | **12-4** |
| $SiO_2$ | 70.70 | 72.13 | 71.29 | 68.83 | 71.70 | 73.24 | 73.66 | 73.50 | 73.40 |
| $TiO_2$ | 0.66 | 0.52 | 0.47 | 0.69 | 0.56 | 0.33 | 0.34 | 0.35 | 0.35 |
| $Al_2O_3$ | 12.50 | 12.20 | 12.25 | 12.37 | 12.37 | 12.32 | 12.38 | 12.39 | 12.42 |
| FeO | 4.50 | 4.47 | 5.63 | 4.47 | 4.01 | 3.13 | 3.48 | 3.59 | 3.77 |
| MnO | 0.09 | 0.05 | 0.10 | 0.14 | 0.12 | 0.07 | 0.09 | 0.08 | 0.06 |
| MgO | 0.69 | 0.42 | 0.31 | 0.84 | 0.57 | 0.36 | 0.21 | 0.16 | 0.20 |
| CaO | 2.71 | 2.58 | 2.40 | 4.98 | 2.72 | 2.16 | 1.35 | 1.49 | 1.33 |
| $Na_2O$ | 3.96 | 3.58 | 4.64 | 3.71 | 3.80 | 4.13 | 4.12 | 4.11 | 4.39 |
| $K_2O$ | 4.04 | 3.98 | 2.84 | 3.83 | 4.05 | 4.22 | 4.35 | 4.30 | 4.05 |
| $P_2O_5$ | 0.14 | 0.08 | 0.08 | 0.14 | 0.11 | 0.04 | 0.03 | 0.03 | 0.03 |
| LOI** | --- | 3.10 | 2.44 | 4.03 | 2.52 | 2.47 | 1.83 | 1.90 | 1.46 |
| Total*** | 97.73 | 95.75 | 96.81 | 94.63 | 96.68 | 96.50 | 96.64 | 97.20 | 97.37 |
| **Trace elements (ppm)** | | | | | | | | | |
| Ni | 4.82 | 6.13 | 6.73 | 5.73 | 9.25 | 4.62 | 2.51 | 2.41 | 3.72 |
| Cr | 3.62 | 5.63 | 4.72 | 5.73 | 3.72 | 3.62 | 2.81 | 2.61 | 2.11 |
| Sc | 9.52 | 8.09 | 7.13 | 9.94 | 8.33 | 5.04 | 4.87 | 4.90 | 5.32 |
| V | 22.81 | 19.80 | 17.69 | 19.80 | 15.48 | 5.73 | 4.52 | 2.21 | 4.02 |
| Ba | 1089.87 | 1086.84 | 917.80 | 1125.55 | 1026.70 | 1149.98 | 1261.96 | 1295.24 | 1247.57 |
| Rb | 88.72 | 84.53 | 70.20 | 81.84 | 88.33 | 90.63 | 96.61 | 94.49 | 89.64 |
| Sr | 142.58 | 103.56 | 113.52 | 203.35 | 174.46 | 73.67 | 73.68 | 83.94 | 88.65 |
| Zr | 594.86 | 690.16 | 659.40 | 639.57 | 651.09 | 719.57 | 732.14 | 725.95 | 729.32 |
| Y | 66.25 | 78.50 | 84.73 | 74.03 | 75.11 | 78.46 | 80.63 | 79.46 | 79.02 |
| Nb | 50.53 | 65.63 | 54.50 | 63.63 | 67.00 | 79.71 | 85.81 | 83.35 | 83.50 |
| Ga | 17.29 | 21.51 | 21.31 | 20.30 | 19.50 | 20.20 | 21.51 | 21.21 | 22.51 |
| Cu | 15.88 | 8.24 | 11.46 | 7.94 | 8.24 | 4.22 | 2.91 | 1.31 | 3.82 |
| Zn | 80.90 | 53.97 | 125.42 | 118.19 | 132.16 | 52.96 | 53.87 | 63.21 | 57.39 |
| Pb | 5.01 | 5.05 | 10.18 | 8.08 | 13.10 | 8.52 | 6.09 | 5.41 | 9.12 |
| La | 60.26 | 74.42 | 66.64 | 67.06 | 69.35 | 82.23 | 85.05 | 83.61 | 82.61 |
| Ce | 129.72 | 161.58 | 144.25 | 145.82 | 152.07 | 175.34 | 177.57 | 174.70 | 172.08 |
| Th | 8.72 | 9.19 | 8.93 | 8.34 | 8.52 | 10.13 | 10.17 | 9.92 | 9.85 |
| Nd | 61.24 | 80.97 | 71.38 | 71.92 | 74.75 | 82.36 | 83.98 | 81.83 | 82.97 |
| U | 2.03 | 2.27 | 2.30 | 2.15 | 2.20 | 2.65 | 2.54 | 2.54 | 2.48 |
| Pr | 15.71 | 20.27 | 17.95 | 18.08 | 18.88 | 21.44 | 21.76 | 21.25 | 21.55 |
| Sm | 12.63 | 17.45 | 15.77 | 15.70 | 16.42 | 17.27 | 17.52 | 17.30 | 17.51 |
| Eu | 2.79 | 4.07 | 3.66 | 3.74 | 3.72 | 3.47 | 3.47 | 3.56 | 3.56 |
| Gd | 11.86 | 16.01 | 14.99 | 14.52 | 14.82 | 15.16 | 15.39 | 15.22 | 15.19 |
| Tb | 2.03 | 2.66 | 2.56 | 2.42 | 2.52 | 2.53 | 2.57 | 2.56 | 2.53 |
| Dy | 12.69 | 15.95 | 16.31 | 14.65 | 15.03 | 15.43 | 15.88 | 15.67 | 15.49 |
| Ho | 2.61 | 3.20 | 3.41 | 2.95 | 3.03 | 3.11 | 3.21 | 3.18 | 3.11 |
| Er | 7.29 | 8.70 | 9.67 | 8.02 | 8.35 | 8.66 | 8.86 | 8.78 | 8.62 |
| Tm | 1.09 | 1.26 | 1.47 | 1.17 | 1.20 | 1.28 | 1.31 | 1.30 | 1.27 |
| Yb | 6.84 | 7.94 | 9.26 | 7.27 | 7.45 | 8.10 | 8.22 | 8.18 | 7.92 |
| Lu | 1.07 | 1.22 | 1.48 | 1.12 | 1.16 | 1.28 | 1.30 | 1.28 | 1.24 |
| Hf | 14.68 | 17.25 | 16.51 | 15.92 | 16.54 | 18.11 | 18.25 | 18.26 | 17.93 |
| Ta | 3.26 | 4.19 | 3.46 | 4.00 | 4.25 | 5.10 | 5.34 | 5.25 | 5.20 |
| Cs | 0.42 | 0.53 | 0.42 | 0.85 | 0.43 | 0.50 | 0.55 | 0.60 | 0.51 |

TABLE 2: GEOCHEMICAL DATA FOR SUBSURFACE RHYOLITE AND GRANITE SAMPLES, CONTINUED

| | Pan Am 1-A Moore (continued) | | | | Pan Am 1-19 Jarman |
|---|---|---|---|---|---|
| | Rhyolite | | | Granite | Rhyolite |
| **Normalized major elements (wt %)*** | | | | | |
| **Sample:** | **12-5** | **12-6** | **12-7** | **12-8** | **23-2** |
| $SiO_2$ | 73.73 | 74.50 | 73.53 | 76.64 | 71.68 |
| $TiO_2$ | 0.34 | 0.38 | 0.43 | 0.21 | 0.70 |
| $Al_2O_3$ | 12.33 | 12.67 | 12.71 | 11.76 | 12.61 |
| FeO | 3.45 | 2.42 | 2.91 | 2.03 | 4.43 |
| MnO | 0.06 | 0.04 | 0.05 | 0.03 | 0.09 |
| MgO | 0.12 | 0.16 | 0.32 | 0.32 | 0.52 |
| CaO | 1.36 | 1.06 | 1.24 | 0.89 | 1.69 |
| $Na_2O$ | 3.88 | 4.08 | 4.28 | 3.43 | 3.96 |
| $K_2O$ | 4.70 | 4.65 | 4.47 | 4.67 | 4.19 |
| $P_2O_5$ | 0.03 | 0.04 | 0.05 | 0.02 | 0.13 |
| LOI** | 1.50 | 1.27 | 1.33 | 1.31 | 1.12 |
| Total*** | 97.66 | 97.47 | 97.77 | 98.89 | 98.62 |
| **Trace elements (ppm)** | | | | | |
| Ni | 2.21 | 10.25 | 2.41 | 4.18 | 2.81 |
| Cr | 3.32 | 33.27 | 3.12 | 15.22 | 3.62 |
| Sc | 4.97 | 5.25 | 6.31 | 2.90 | 9.48 |
| V | 4.62 | 4.12 | 5.73 | 7.16 | 14.07 |
| Ba | 1173.70 | 1247.72 | 1227.63 | 589.23 | 883.87 |
| Rb | 109.50 | 110.18 | 101.96 | 134.73 | 91.75 |
| Sr | 74.34 | 67.63 | 74.94 | 38.57 | 121.79 |
| Zr | 736.85 | 633.01 | 709.28 | 379.40 | 634.34 |
| Y | 80.33 | 73.46 | 75.06 | 64.11 | 70.51 |
| Nb | 85.11 | 74.54 | 75.93 | 87.92 | 59.74 |
| Ga | 20.30 | 18.99 | 19.30 | 20.90 | 16.68 |
| Cu | 4.72 | 2.81 | 2.41 | 10.55 | 7.84 |
| Zn | 41.21 | 39.60 | 65.02 | 29.65 | 89.85 |
| Pb | 7.44 | 6.01 | 7.16 | 5.62 | 10.27 |
| La | 86.13 | 78.83 | 79.09 | 98.28 | 67.05 |
| Ce | 179.21 | 161.44 | 163.35 | 188.74 | 143.37 |
| Th | 10.10 | 10.96 | 10.69 | 15.38 | 9.06 |
| Nd | 86.30 | 74.68 | 75.49 | 79.43 | 68.70 |
| U | 2.51 | 2.64 | 2.53 | 3.53 | 2.18 |
| Pr | 22.31 | 19.74 | 19.91 | 22.09 | 17.72 |
| Sm | 17.84 | 15.04 | 15.46 | 14.81 | 14.45 |
| Eu | 3.53 | 2.60 | 2.90 | 1.36 | 3.05 |
| Gd | 15.60 | 13.33 | 13.83 | 12.13 | 13.08 |
| Tb | 2.61 | 2.26 | 2.32 | 2.00 | 2.18 |
| Dy | 15.69 | 13.96 | 14.31 | 12.10 | 13.42 |
| Ho | 3.17 | 2.83 | 2.91 | 2.49 | 2.76 |
| Er | 8.75 | 7.96 | 8.04 | 6.90 | 7.61 |
| Tm | 1.29 | 1.18 | 1.17 | 1.03 | 1.12 |
| Yb | 8.09 | 7.37 | 7.48 | 6.56 | 7.06 |
| Lu | 1.27 | 1.16 | 1.17 | 1.04 | 1.11 |
| Hf | 18.17 | 16.26 | 17.49 | 10.19 | 15.51 |
| Ta | 5.32 | 4.80 | 4.81 | 5.74 | 3.80 |
| Cs | 0.75 | 0.60 | 0.56 | 0.59 | 0.21 |

* Major elements are normalized to 100% on a volatile-free basis

** Loss on ignition ***Total before normalization

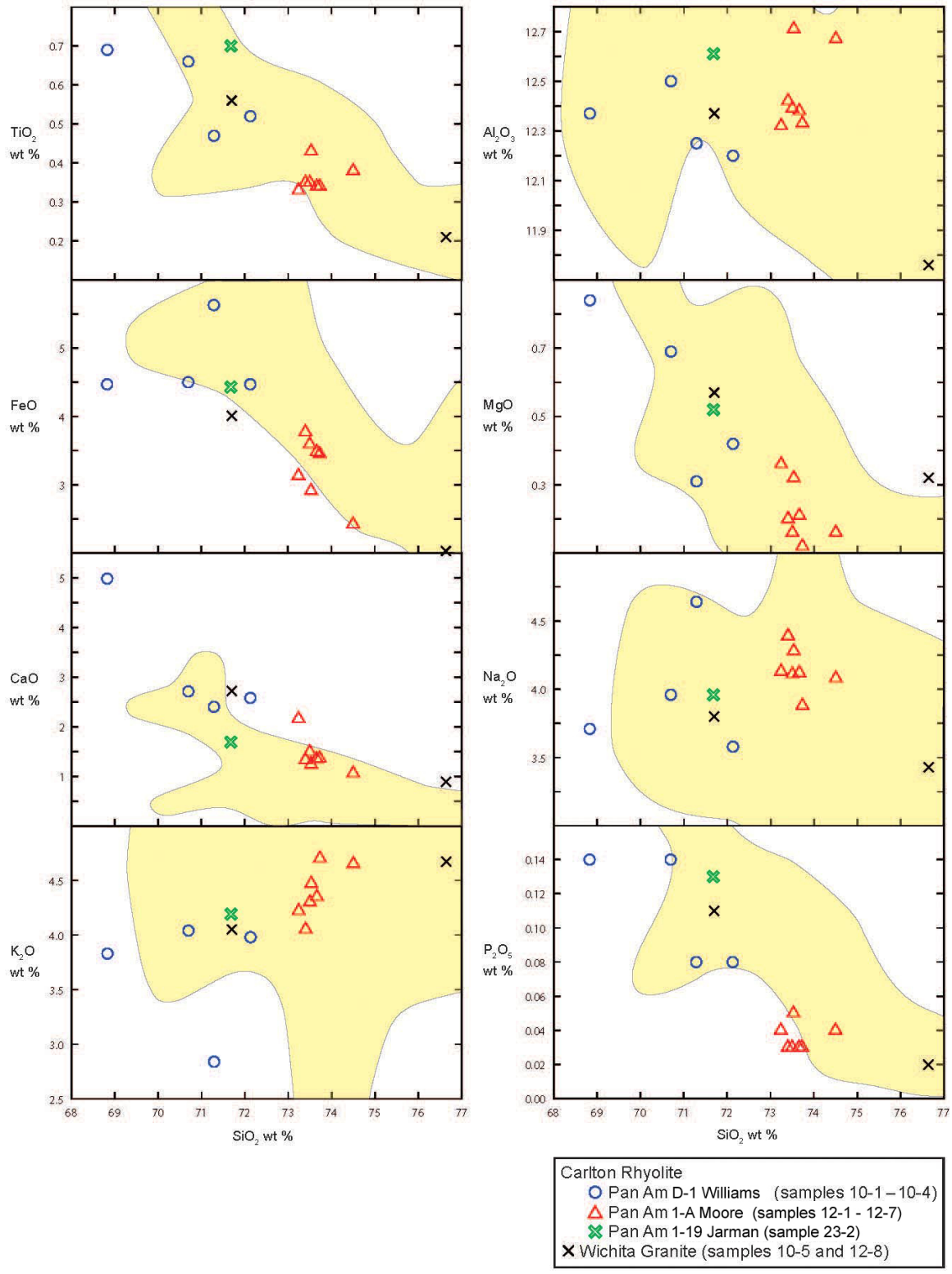


**Figure 13. Major oxides for subsurface rhyolite samples plotted on Harker variation diagrams. Yellow fields represent data for Carlton Rhyolite in the Wichita and Arbuckle Mountains (Hanson and Eschberger paper, this guidebook). Fields look unusual on some diagrams compared to those in Hanson and Eschberger paper (this guidebook) because of differences in the y-axis scale.**

alteration is lacking in thin section, some of the scatter in these plots probably reflects secondary disturbance of the major elements. The alkalis show more scatter, which reflects the general mobility of these elements during alteration and is consistent with the presence of chessboard albite in some samples.

The seven samples from the Pan Am 1-A Moore well show more evolved compositions on the Harker diagrams than the rhyolite samples from the other two wells. The Pan Am 1-A Moore samples are also fairly tightly clustered. According to the lithologic log for this well (Fig. 2), the samples come from several different flows separated in places by volcaniclastic interbeds, but the general similarity in the major-element compositions of the flows suggests that they tapped parts of a single magma chamber that maintained a fairly uniform composition for some length of time.

On standard trace-element diagrams all the samples fall within fields defined by data from other parts of the Carlton Rhyolite (Fig. 14). The Pan Am 1-A Moore samples plot well within the peralkaline field in Figure 14A, in keeping with their somewhat more fractionated patterns in Figure 14D. REE patterns for all the subsurface rhyolite samples (Fig. 14E) are very similar, however, which implies that they had comparable petrogenetic histories. Granite sample 12-8 shows the most fractionated pattern in Figure 14D and a more pronounced negative Eu anomaly than the other samples (Fig. 14E), in keeping with its more evolved major-element composition.

## SYN-RIFT SEDIMENTATION

Although rare in outcrop in southern Oklahoma, syn-rift sedimentary strata have been modeled in seismic velocity studies of the deepest part of the Anadarko Basin in southwestern Oklahoma (Keller and Stephenson, 2007; Buckey, this guidebook). In the Arbuckle wells, substantial accumulations of three different types of syn-rift sedimentary deposits are present and are discussed below.

### Rhyolitic Volcaniclastic Sedimentary Rocks

Texturally immature rhyolitic volcaniclastic sedimentary rocks form intervals as thick as 98 m and are intercalated with rhyolite and basalt lavas in several of the Arbuckle wells. By far the thickest accumulation of these rocks occurs in the Frankfort 1 Sparks Ranch well, where the volcaniclastic strata have a cumulative thickness of 1021 m (Fig. 2). This is the thickest sequence of volcaniclastic sedimentary rocks documented anywhere in the Southern Oklahoma Aulacogen.

Twenty-two thin sections of cuttings from different depths in the Frankfort 1 Sparks Ranch well reveal a variety of clast types and textures in these rocks. Most of the cuttings contain angular to subrounded, silt- to sand-size rhyolite lithic grains and loose crystals and crystal fragments of volcanic quartz, plagioclase, and alkali feldspar (Figs. 15A and 15B). Sorting is typically very poor with coarser sand-size grains in a silt-rich matrix (Fig. 15A). The lithic grains show the same range of groundmass textures that is present in lavas in other parts of the Carlton Rhyolite Group, including perlitic, spherulitic, amygdaloidal, and microcrystalline with tridymite needles. Some cuttings are single pieces of rhyolite that we interpret as gravel-size lithic clasts; in some cases, the silt- and sand-size matrix to these grains is still preserved on the margins of the cuttings. Phenocrysts in rhyolite lithic grains include quartz, feldspar, and mafic silicates replaced by green clays. In a few intervals, sand-size basaltic particles occur in small amounts and consist of sideromelane replaced by green clay (Fig. 15A). The basaltic particles are typically angular to subrounded, but rarely their margins are partly defined by broken bubble walls, indicating very limited sedimentary transport. It is likely that these particles represent ash that was derived from explosive basaltic phreatomagmatic eruptions and that was intermixed with rhyolitic debris prior to or during transport and deposition.

Ham et al. (1964) presented a detailed lithologic log for the Frankfort 1 Sparks Ranch well, but our interpretations differ significantly from theirs. They documented several intervals of “rhyolite tuff” in the well and one interval of rhyolite agglomerate but considered most of the Carlton Rhyolite section to be rhyolite lava. We instead interpret most of the rhyolitic material in this well to be volcanic debris that was reworked by normal sedimentary processes. The difference in interpretations may partly reflect advances in the understanding of volcanic and volcaniclastic textures since the pioneering work of Ham et al. (1964).

We have also examined thin sections of thinner intervals of rhyolitic volcaniclastic rocks penetrated in the Pan Am 1 Newberry and Pan Am 1-19 Jarman wells, where the volcaniclastic rocks are interbedded with basalt or rhyolite lavas (Fig. 2). Where the volcaniclastic rocks are in direct contact with rhyolite lavas, it is not always possible to determine from the cuttings whether they represent flow breccia at the base or top of flows or volcanic debris reworked by sedimentary processes. We can confidently ascribe a sedimentary origin to cuttings consisting of polymict rhyolitic sandstones or sandy pebble conglomerates

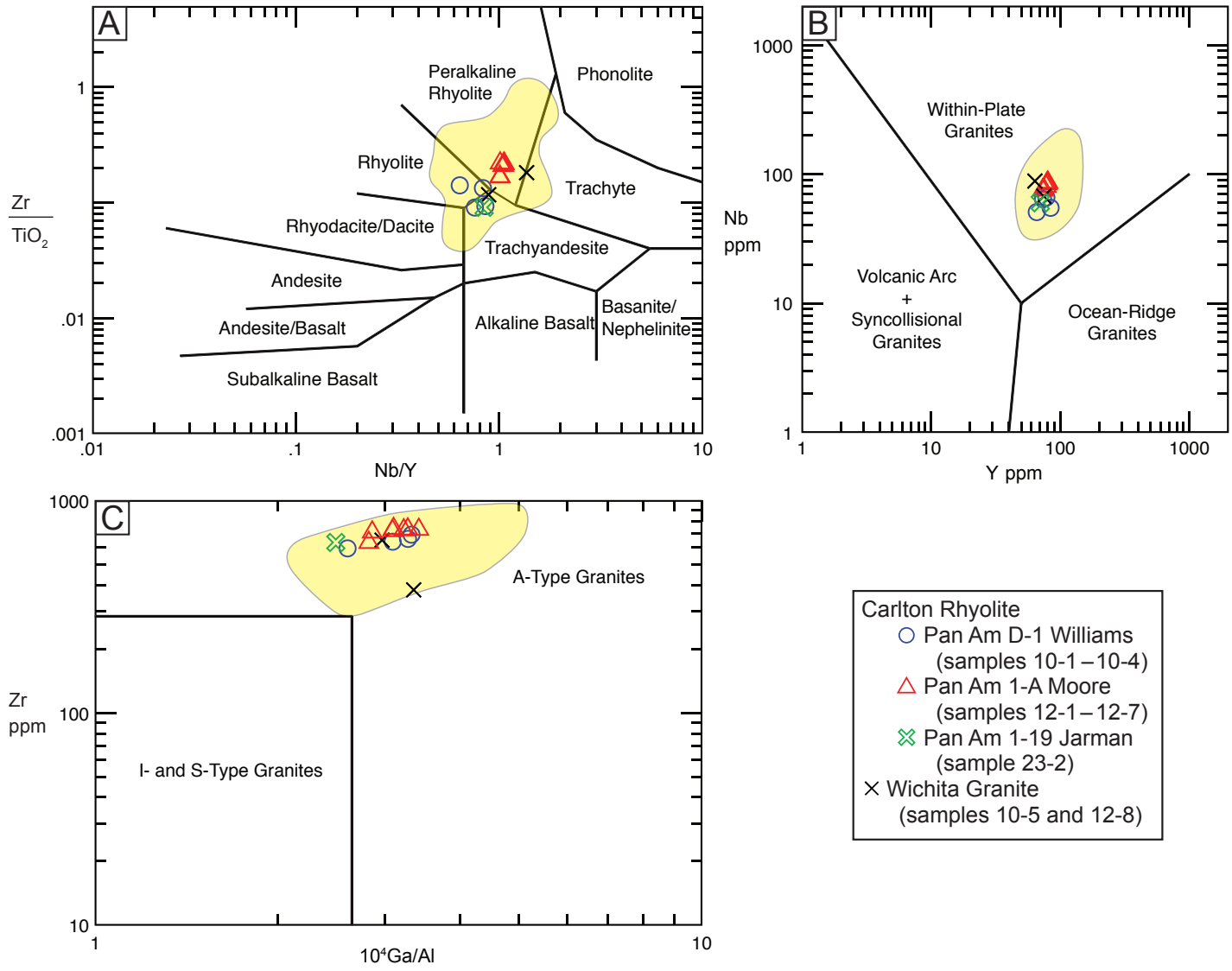


**Figure 14. Trace-element data for subsurface rhyolites plotted on various diagrams. (A) $Zr/TiO_2$ vs. Nb/Y classification diagram of Winchester and Floyd (1977). (B) Nb vs. Y discrimination diagram of Pearce et al. (1984). (C) Zr vs. $10^4$Ga/Al discrimination diagram of Whalen et al. (1987). (D) and (E) Multi-element and REE diagrams; normalization values from Sun and McDonough (1989). Yellow fields represent data for Carlton Rhyolite in the Wichita and Arbuckle Mountains (Hanson and Eschberger paper, this guidebook).**

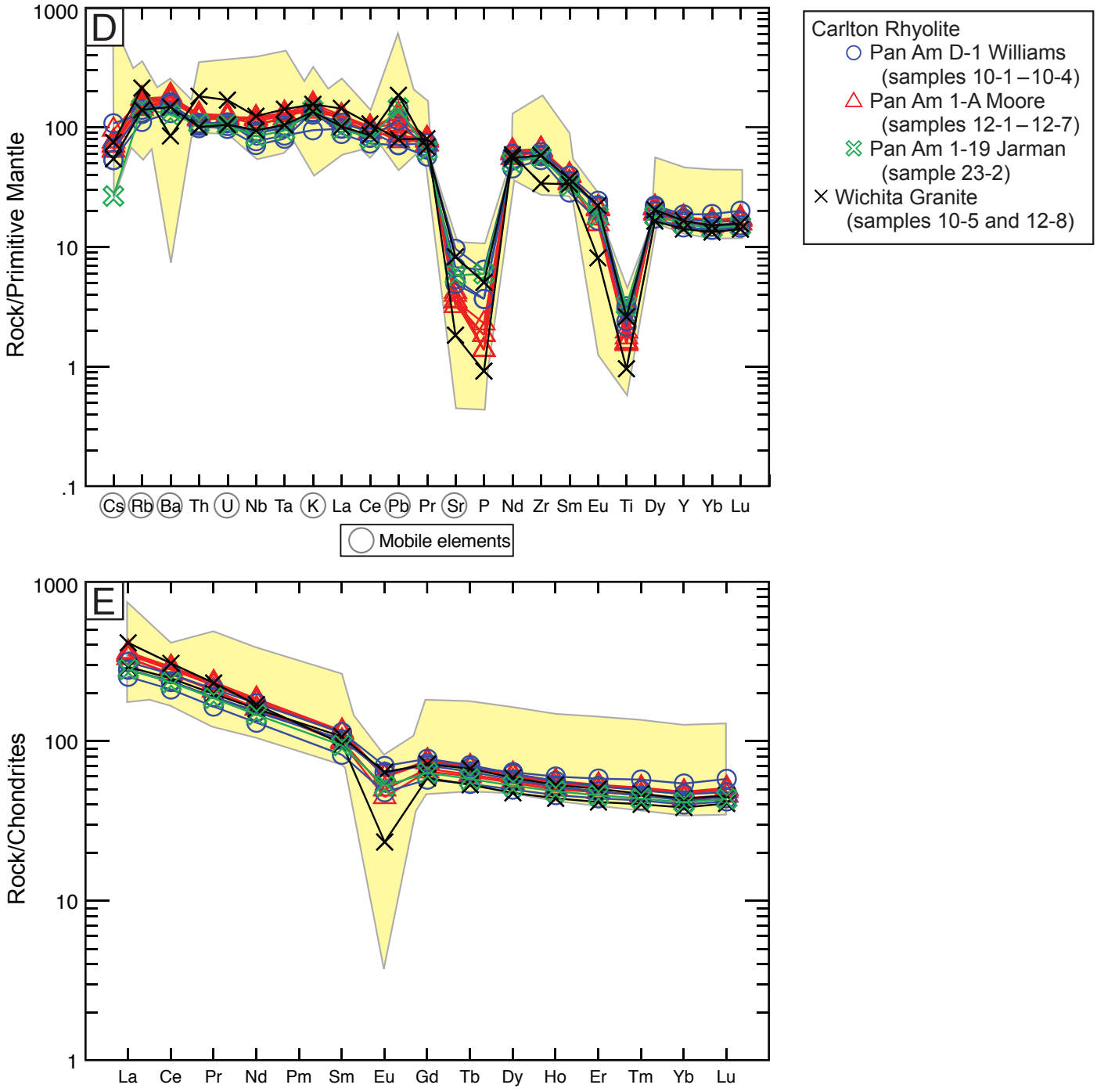


**Figure 14 continued.**

or where rounded lithic grains are present (e.g., Fig. 15C). One such interval (1924 m to 1927 m) in the Pan Am 1-19 Jarman contains minor amounts of tricuspate bubble-wall shards and compacted pumice intermixed with sand-size rhyolitic crystal and lithic grains (Fig. 15D). The shards and pumice may indicate a minor component of reworked pyroclastic material but could conceivably also be derived from pumiceous layers within rhyolite lavas.

### Non-Volcaniclastic Sedimentary Rocks

The Pan Am 1-19 Jarman well contains a thick clastic section interpreted as a fan delta prograding into the rift from its northern margin. This section was subsequently covered by later volcanic eruptions (Fig. 16) and represents the only known significant intercalation of terrigenous sedimentary rocks within the volcanic succession in the rift zone. The primary lithology is white to tan, arkosic to subarkosic sandstone with less-common beds of rhyolitic volcaniclastic sedimentary rocks and tuffaceous mudstone. The arkosic sediments contain two populations of clastic grains inferred to have been derived from Proterozoic crystalline rocks exposed outside the rift zone: a predominant fraction of well-sorted, fine-grained quartz and feldspar possibly derived from granitic or gneissic sources and a lesser amount of coarse-grained, subrounded to well-rounded quartz and feldspar grains plus lithic fragments which indicate derivation from mesozonal granites (Figs. 16A and 16C). Coarse feldspar grains consist of microcline and perthite, and finer feldspar grains comprise orthoclase, microcline, and plagioclase. The coarse quartz grains are commonly polycrystalline. Quartz grains from both size fractions were typically partially coated with authigenic clay minerals early in the diagenetic sequence and subsequently overgrown with silica cement in optical continuity with the original grain (Fig. 16B). Hematite cement is present in significant quantities in two horizons (3710 ft to 3782 ft and 4508 ft to 4615 ft in Fig. 16) and in minor amounts throughout the section. Openwork texture in hematite-cemented sandstones (Fig. 16D) suggests that the hematite formed prior to significant burial and compaction. Hematite cement is also observed coating many of the coarse, rounded to well-rounded quartz grains, and some late-stage carbonate cement is present.

### Post-Volcanic Sedimentary Deposits

The Reagan Sandstone that unconformably overlies the Cambrian volcanic rocks in southern Oklahoma is characterized by hematite-cemented, poorly sorted arkosic fluvial conglomerate and sandstone that grades upward into glauconitic marine quartz sandstone, the upper part of which contains Late Cambrian trilobites (Stitt, 1973). In the Frankfort 1 Sparks Ranch well, an anomalous, 64-m-thick white to tan arkosic sandstone is present between the volcanic erosional surface and the overlying arkosic, hematite-cemented fluvial facies typical of the basal Reagan Sandstone (Fig. 17). The arkosic sandstone is petrologically identical to the fan-delta deposits in the Pan Am 1-19 Jarman well discussed above and lacks the rhyolitic lithic fragments found in the overlying Reagan Sandstone where that unit rests on Cambrian volcanic rocks. The Frankfort 1 Sparks Ranch well is located approximately 7 km closer to the rift axis than any other well studied to date, and the unit beneath the Reagan is interpreted to record fluvial redistribution of fan-delta sediments similar to those present in Pan Am 1-19 Jarman and originating from outside the rift. Since the fan-delta deposits in the 1-19 Jarman well were covered by later volcanism, the anomalous unit in the 1 Sparks Ranch well raises the possibility of multiple sediment sources flowing into the rift. This fluvial unit, as well as the thick volcaniclastic deposits discussed above from the same well, suggest that at least parts of the rift in the Arbuckle area were not over-filled with volcanic deposits, as suggested by Ham et al. (1964), but instead may have retained a negative topographic profile during much of its pre-Reagan history.

Based on the limited available data, sediment transport into the rift from the adjacent craton may not have been widespread. However, it is possible that additional examples of craton-derived clastic accumulations remain to be discovered in other parts of the rift not penetrated by drilling.

## GRANITE

Southern Oklahoma Aulacogen magmatism includes voluminous intrusions belonging to the Wichita Granite Group (WGG). These are exposed at the surface throughout the Wichita Mountains and extend in the subsurface to the Arbuckle Mountains (Ham et al., 1964). Exposures of individual granite units are widely distributed, and a few examples display a near-horizontal base that implies a sheet or tabular geometry. They are alkali-feldspar granites, and their alkali feldspar grains are invariably perthitic. A few WGG units contain minor amounts of plagioclase. All contain titaniferous oxides ± biotite ± amphibole. Hornblende is the dominant amphibole, but sodic amphiboles are present in some units. The mafic and accessory minerals are

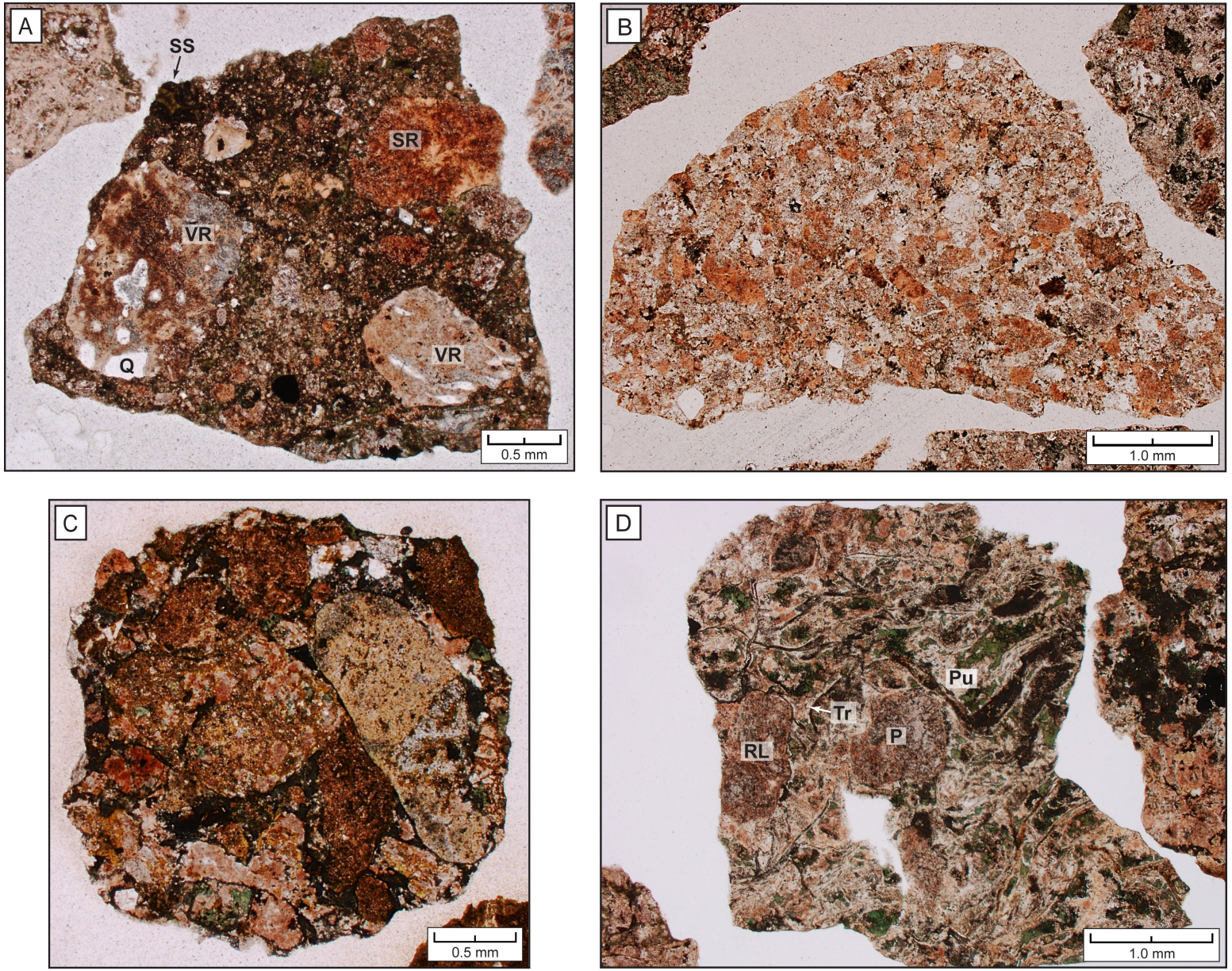


**Figure 15. Photomicrographs of rhyolitic volcaniclastic sedimentary rocks, all in plane light; locations in wells are shown in Figure 2. (A) Frankfort 1 Sparks Ranch. Poorly sorted rhyolitic sandstone with sand-size grains in a silt-rich matrix. *SS*: altered basaltic sideromelane shard; *SR*: spherulitic rhyolite grain; *VR*: vesicular rhyolite grains; *Q*: quartz phenocryst in vesicular rhyolite grain. (B) Frankfort 1 Sparks Ranch. Rhyolitic sandstone containing angular to subangular grains of quartz, feldspar, and rhyolite. (C) Pan Am 1-19 Jarman. Rhyolitic sandstone containing subrounded to well-rounded lithic grains. (D) Pan Am 1-19 Jarman. Rhyolitic sandstone containing tricuspate shards (*Tr*) and compacted pumice (*Pu*); *P*: plagioclase grain; *RL*: rhyolite lithic grain.**

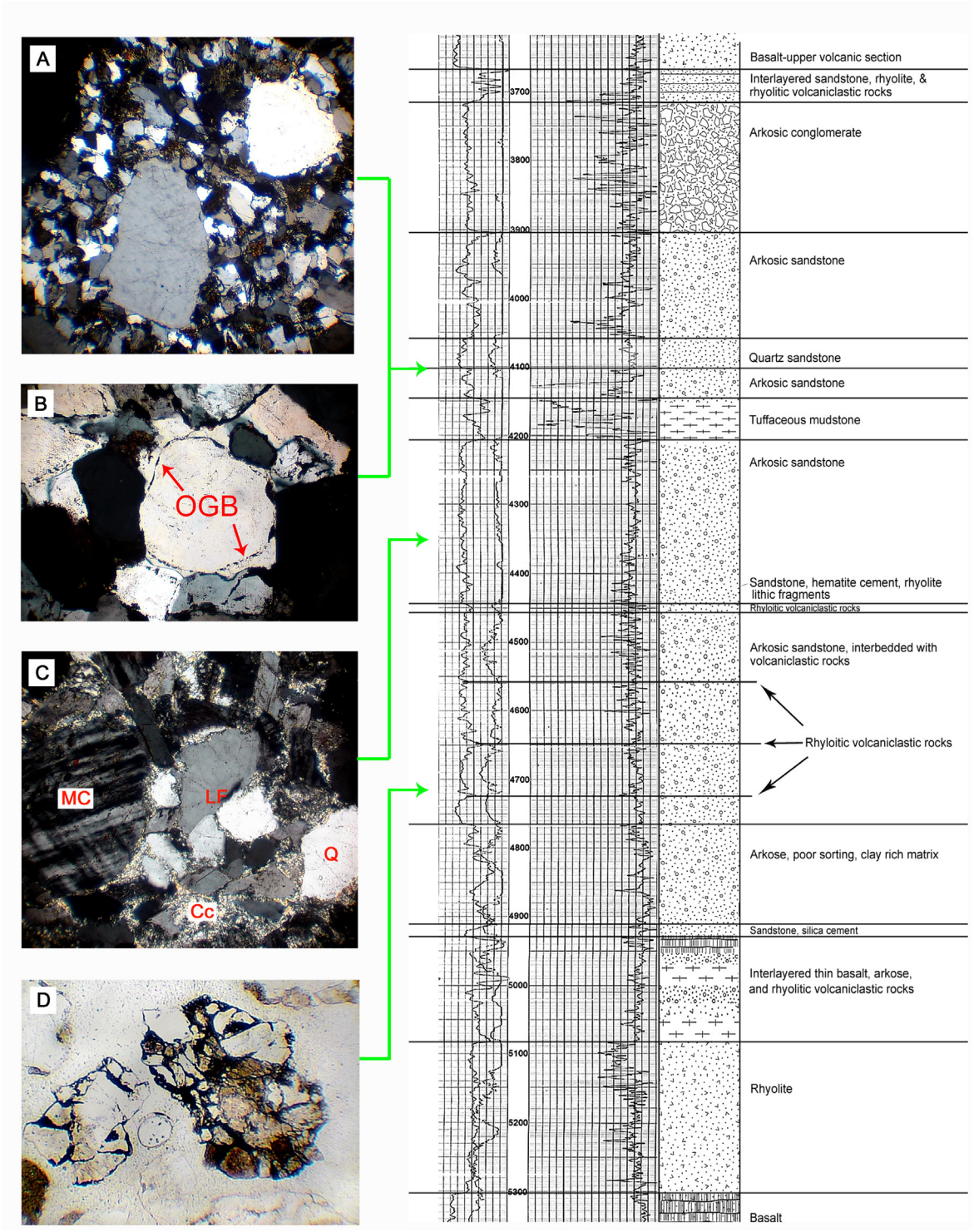


**Figure 16. Syn-rift fan-delta clastic section in the Pan Am 1-19 Jarman well. (A) Bimodal sorting of fine-grained quartz and feldspar and coarse, subrounded quartz grains; crossed polars, width of field of view is 2.62 mm. (B) Coarse, well-rounded quartz grain with silica cement deposited on the grain boundary surface in optical continuity with the grain. The original grain boundary (*OGB*) is delineated by authigenic clay deposited prior to silica cementation. Crossed polars, width of field of view is 0.98 mm. (C) Coarse-grained granitic debris; crossed polars, width of field of view is 0.91 mm; *MC*: microcline grain; *LF*: granitic lithic fragment; *Q*: quartz grain; *Cc*: carbonate cement. (D) Sandstone containing quartz, feldspar, and granitic lithic fragments cemented by hematite (opaque); plane light, width of field of view is 1.70 mm. Texture indicates that hematite cement formed before compaction.**

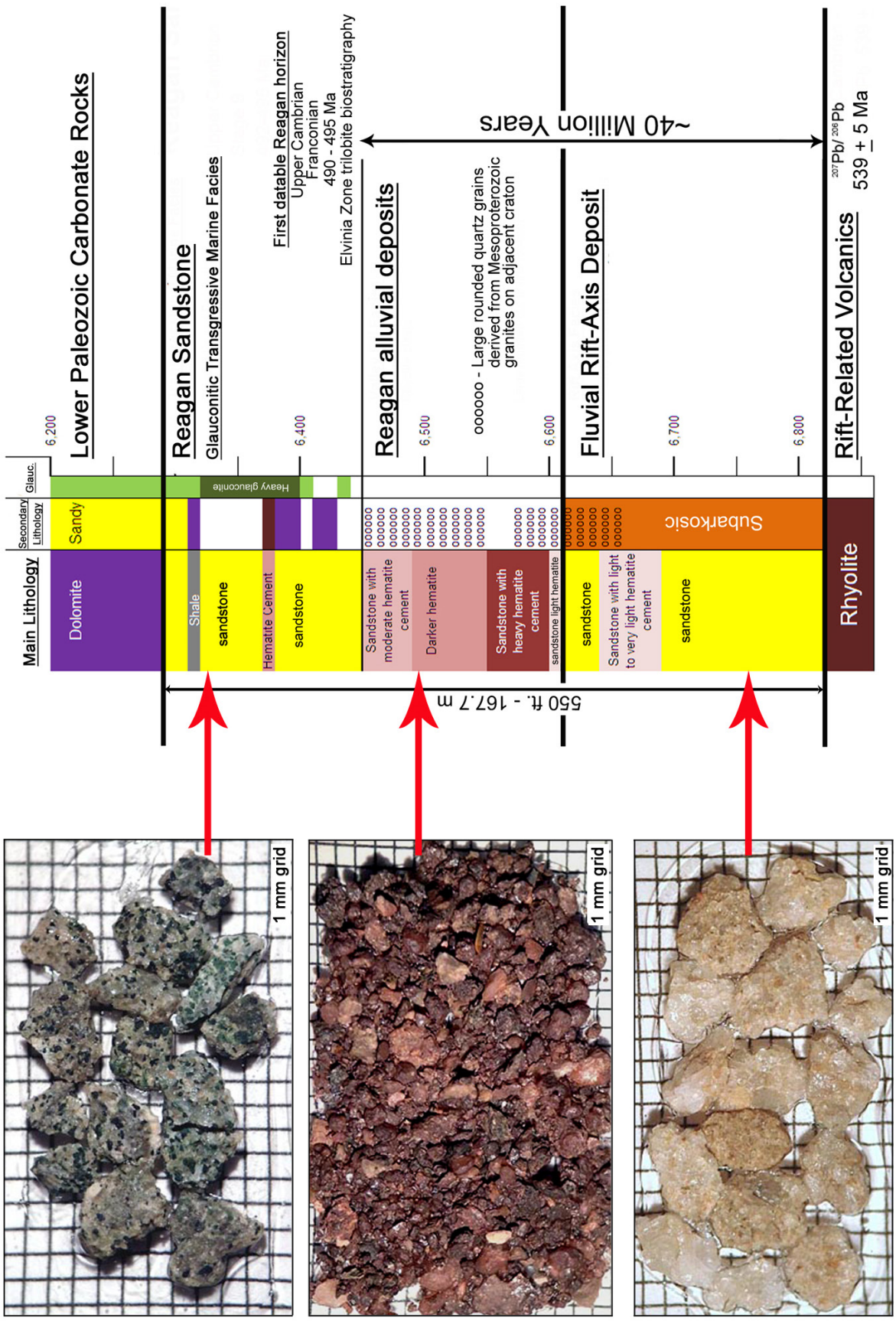


**Figure 17. Basal Paleozoic sedimentary section in the Frankfort 1 Sparks Ranch well. The lowermost sandstone unit is petrologically consistent with redistribution of the fan-delta sediments seen in the Pan Am Jarman well (Fig. 16) and lacks the rhyolite fragments found in basal Reagan fluvial deposits. Age for rift-related volcanic rocks is a weighted mean $^{207}Pb/^{206}Pb$ zircon age for a rhyolite in the East Timbered Hills in the Arbuckles (Thomas et al., 2012). Age for Franconian is based on comparison between Cambrian time scales in Harland et al. (1990) and Gradstein et al. (2012).**

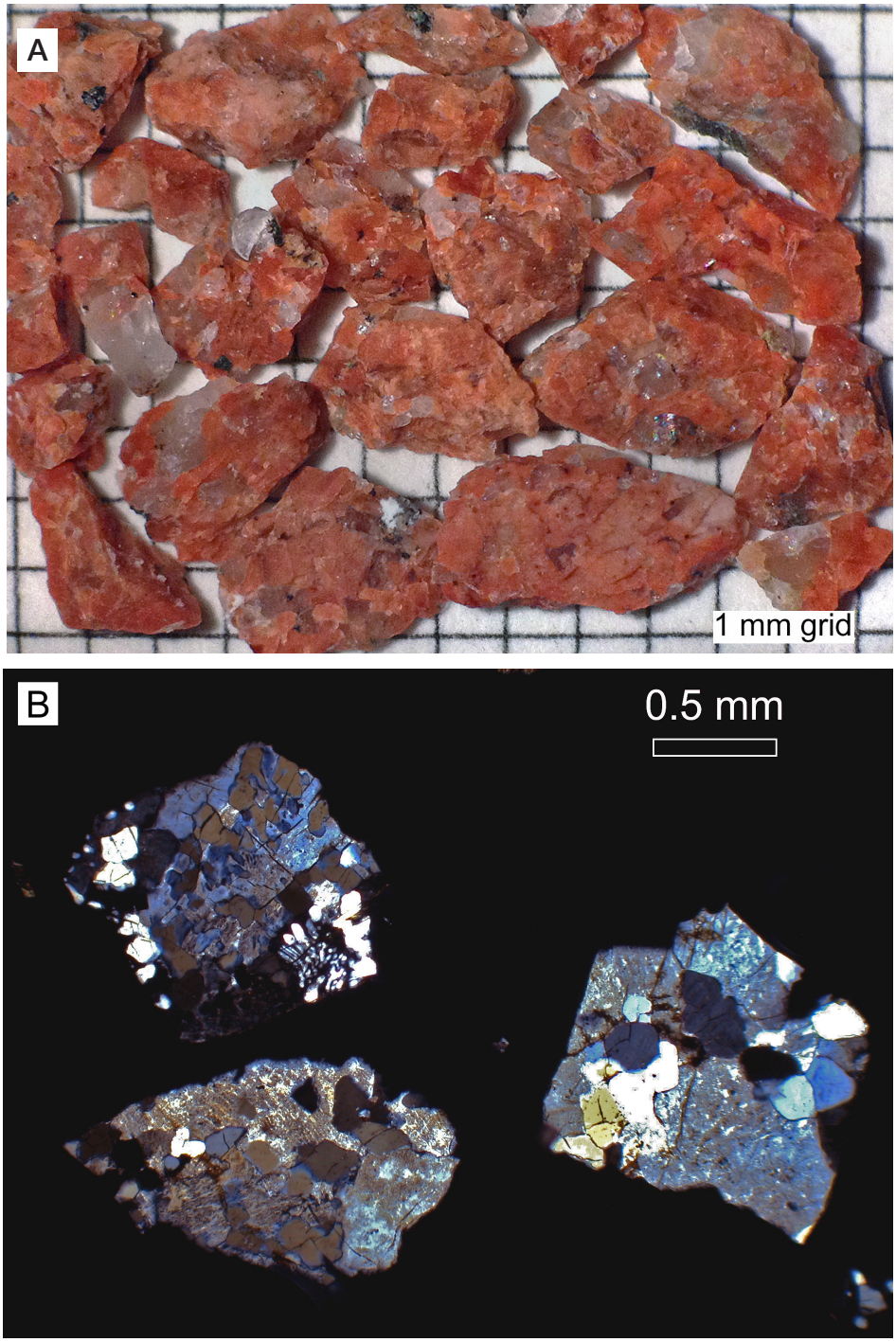


**Figure 18. (A) Cuttings of red alkali feldspar granite from the Kaiser Francis 1 Chapman well; see Figure 2 for sample location. Clear quartz grains are visible; mafic minerals are elongate and glomerocrystic. (B) Photomicrograph (crossed polars) of granite cuttings from the Hamilton Brothers 1-18A Turner Falls well. Turbid grains of strongly perthitic alkali feldspar granophyre and phenocrysts dominate the samples. Clear quartz grains exhibit typical granophyre optical extinction in thin section.**

typically glomerocrystic and occur as enclaves in some units. Individual units are either a fine- to medium-grained porphyry with a granophyric to hypidiomorphic-granular texture or less typically coarser-grained seriate; granophyric texture, however, is characteristic of the WGG as a whole (Price paper, this guidebook). Most of the granites have brick- to orange-red weathered surfaces that may lighten with depth (Price et al., 1998; Hamilton et al., this guidebook).

The sheet granites exposed in the Wichita Mountains are generally considered to have been primarily emplaced between the eroded top of the Glen Mountains Layered Complex and the overlying volcanic pile (Hogan and Gilbert, 1995, 1997; Price paper, this guidebook). No gabbros have been encountered in wells in the Arbuckle area, emphasizing a major difference in the large-scale igneous stratigraphy between this part of the aulacogen and the Wichita Mountains area farther west (see also Ham et al., 1964).

Several significant granite intrusions are evident from the subsurface data (Fig. 2). Granites are found as sheets or sills of variable thickness throughout the igneous section, with the thickest occurrence (1.3 km) being present in the John A. Taylor 1 Morrow well. The base of the granite body in that well is truncated by the Washita Valley Fault so the total thickness of the granite is unknown. Chilled margins extending 10 m to 20 m into the thickest granite bodies are commonly observed. Abundant microgranites occur as thinner intrusive sheets and can be distinguished from the rhyolites by the presence of granophyric texture in thin section.

We examined granite cuttings in detail from four wells, including the John A. Taylor 1 Morrow, Frankfort 1 Sparks Ranch and Hamilton Brothers 1-18A Turner Falls wells shown in Figure 2 and the Kaiser Francis 1 Chapman well lo-

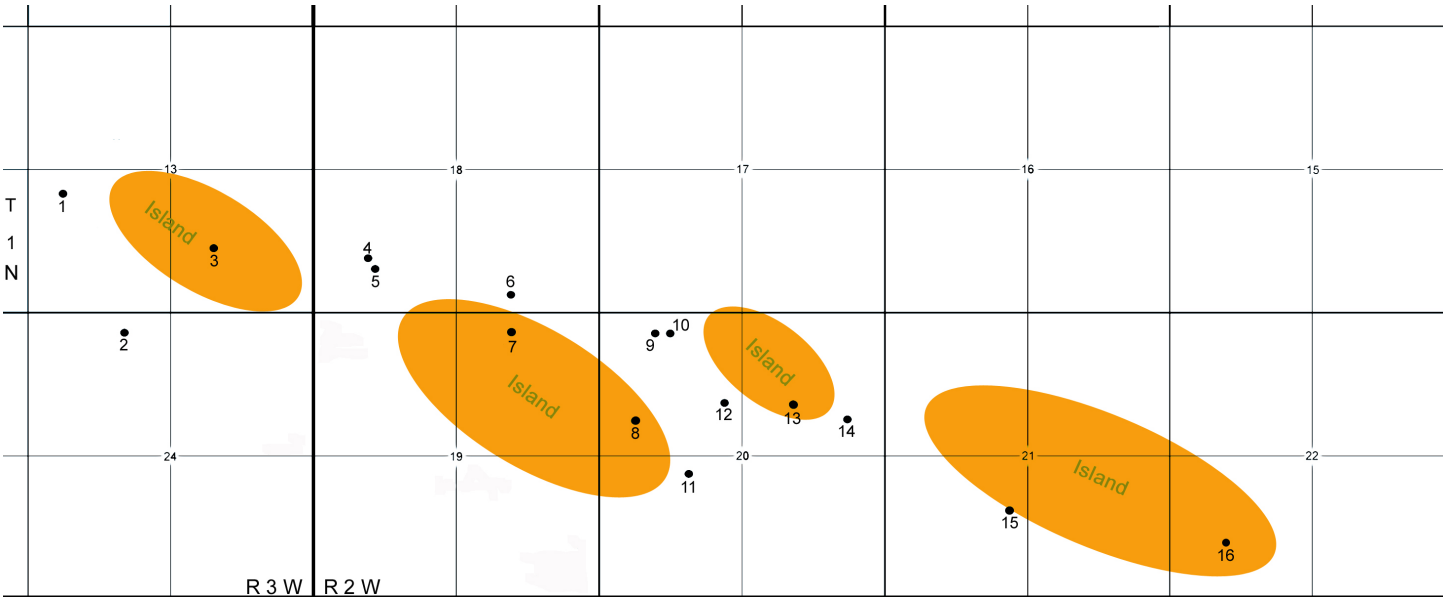


**Figure 19. Islands of rift-related volcanic rocks emergent during Reagan Sandstone deposition as indicated by missing Reagan section at the unconformity surface.**

cated southeast of the East Timbered Hills in the Arbuckle Mountains and shown in Figure 19 in Eschberger et al. paper (this guidebook).

Ham et al. (1964) previously studied granite penetrated in the lower part of the Frankfort 1 Sparks Ranch well and characterized these rocks as medium-grained micrographic granite porphyry dominated by perthite and quartz. According to their descriptions, primary and secondary mafic silicates include chlorite and rare epidote in the upper part of the granite interval, clinopyroxene with trace amphibole and epidote in the intermediate-depth cuttings, and amphibole and biotite with trace chlorite, augite and epidote in the deepest cuttings. Our observations on the granite cuttings from this well are broadly in accord with those of Ham et al. (1964). The mafic minerals are elongate (likely amphibole or pseudomorphs of that phase) and are glomerocrystic at all three depths. The abundance of mafic minerals decreases with depth and the overall color becomes lighter. Chips from the deepest sample include fragments of white feldspar phenocrysts. The change in color with depth is not the result of weathering (in contrast to the color change shown by some of the WGG where it is exposed in the Wichita Mountains) and may reflect a change in bulk composition of the granite intrusion; further work is needed to resolve this question.

Cuttings from the granite interval in the Kaiser Francis 1 Chapman well are pink-red to light-pink or white alkali feldspar granite with relatively large (as large as 3 mm) quartz grains and glomerocrystic mafic minerals (Fig. 18A). Granite cuttings from the 1 Morrow and 1-18A Turner Falls wells are generally similar in appearance to those from the Kaiser Francis 1 Chapman well. Chips with granophyre nucleated on medium-grained phenocrysts of perthitic alkali feldspar are present at each sampled depth in the John A. Taylor 1 Morrow and Hamilton Brothers 1-18A Turner Falls wells. Thin sections of samples from these two wells reveal additional details.

Chips of alkali feldspar granite in the John A. Taylor 1 Morrow contain optically clear quartz and perthitic alkali feldspar and 2 to 3% mafic minerals in very fine to medium quasi-cuneiform granophyre. The textures in two other thin sections from this well are granophyric in one thin section and contain hypidiomorphic feldspars and quartz in the other. Partially altered biotite occurs as patchy intergrowths with quartz, feldspar, opaques (presumably hematite) and accessory minerals, including euhedral titanite.

Granite chips from the Hamilton Brothers 1-18A Turner Falls well (Fig. 18B) contain a mixture of fine (0.01 mm) radiating vermicular granophyric quartz and coarser (0.5 mm) granophyric quartz. Feldspar phenocrysts have relatively large exsolved domains in the cuttings, but the percentage of phenocrysts appears to decrease at depth. Cuttings (GR-1) contain granophyre but also contain a hypidiomorphic granite with euhedral perthitic alkali feldspar not seen elsewhere in this well or in the other wells. This odd texture is not seen in sample GR-2, at which depth all chips are generally gra-

nophyric but with a coarser grain size. At all depths, partially altered biotite occurs as patchy intergrowths with quartz, feldspar, opaque minerals, and accessory titanite and zircon. Small white micas, the alteration products of alkali feldspar, are present at all sample depths.

One of the main conclusions of this part of our subsurface research is that the granite intrusions in all four of the studied wells are, in general, strikingly similar in grain size, texture, mineral content, and color to examples from the WGG exposed in the Wichita Mountains. All are granophyric alkali-feldspar granites containing little or no plagioclase. Our results further emphasize the overall uniformity of the WGG throughout the Southern Oklahoma Aulacogen.

## POST-VOLCANIC TOPOGRAPHY

Following active volcanism and an erosional period of up to ~ 40 Ma, the Reagan Sandstone was deposited at the beginning of a broad transgression onto the craton. Typical Reagan sections include a basal fluvial conglomerate that grades upward into glauconitic marine quartz sandstones (discussed earlier). In the Wichita Mountains area, the topographic relief on the volcanic surface is large enough that six paleo-islands of Carlton Rhyolite that were not inundated by Reagan clastics have been identified in outcrops in southwestern Oklahoma (Donovan, 2000; Donovan and Bucheit, 2000). The islands are characterized by the lack of Reagan siliciclastics at the unconformity, so that stratigraphically higher carbonate units lie on the rhyolite erosional surface. Using biostratigraphic techniques to identify horizons in the carbonates in contact with the rhyolite highs, the maximum relief of the islands is ~330 m (Donovan, 2000; Donovan and Bucheit, 2000). These islands occur along a linear outcrop area ~40 km in length from Bally Mountain to the Blue Creek Canyon area in the Slick Hills north of the main mass of the Wichita Mountains and have been informally named the Southern Oklahoma archipelago (Donovan, 2000).

In the Arbuckle Mountains, no rhyolite paleo-islands of the type recognized in the Wichitas appear to be present in outcrops of the unconformity, although granite paleo-islands do occur in the eastern Arbuckle Mountains where the Reagan unconformably overlies Mesoproterozoic basement (Ham, 1973). Closely spaced well data from the wells studied in the present project, however, has revealed four islands scattered across a 7-km trend (Fig. 19) where the Reagan is absent and the volcanic rocks are unconformably overlain by post-Reagan lower Paleozoic carbonate rocks. Recognition of these paleo-islands in the western Arbuckle area suggests that the unconformity surface may have been irregular over large parts of its extent. These topographic highs must have strongly influenced the distribution of post-rift sediments, the generation of thick sequences of Reagan alluvium (discussed earlier in this paper), and the distribution of craton-generated siliciclastic marine sediments during accumulation of the Reagan transgressional sequence.

## REFERENCES CITED


Bryan, W.B., 1972, Morphology of quench crystals in submarine basalts: Journal of Geophysical Research, v. 77, p. 5812-5819.

Bulen, C.L., 2012, The role of magmatism in the evolution of the Cambrian Southern Oklahoma rift zone: Geochemical constraints on the mafic-intermediate rocks in the Arbuckle Mountains, Oklahoma [M.S. thesis]: Manhattan, Kansas, Kansas State University, 87 p.

Denison, R.E., 1995, Significance of air-photograph linears in the basement rocks of the Arbuckle Mountains, *in* Johnson, K.S., ed., Structural Styles in the Southern Midcontinent, 1992 symposium: Oklahoma Geological Survey Circular 97, p. 119-131.

Donovan, R.N., 2000, Sediment transport around islands, ancient and modern: Examples from the west coast of Scotland and southwestern Oklahoma, *in* Johnson, K.S., ed., Marine Clastics in the Southern Midcontinent, 1997 Symposium: Oklahoma Geological Survey Circular 103, p. 19-23.

Donovan, R.N., and Bucheit, A.K., 2000, Marine facies and islands in the Reagan Formation (Upper Cambrian) in the Slick Hills, southwestern Oklahoma, *in* Johnson, K.S., ed., Marine Clastics in the Southern Midcontinent, 1997 Symposium: Oklahoma Geological Survey Circular 103, p. 25-37.

Eschberger, A.M., 2012, Volcanological and geochemical studies of Cambrian rift-related igneous rocks in the western Arbuckle Mountains, southern Oklahoma [M.S. thesis]: Fort Worth, Texas, Texas Christian University, 191 p.

Gradstein, F.M., Ogg, J.G., Schmitz, M.D., and Ogg, G.M., 2012, The Geologic Time Scale 2012: Amsterdam, Elsevier, 1144 p.

Ham, W.E., 1973, Regional Geology of the Arbuckle Mountains, Oklahoma: Oklahoma Geological Survey Special Publication 73-3, 61 p.

Ham, W.E., Denison, R.E., and Merritt, C.A., 1964, Basement Rocks and Structural Evolution of Southern Oklahoma: Oklahoma Geological Survey Bulletin 95, 302 p.

Hanson, R.E., Puckett, R.E., Jr., Keller, G.R., Brueseke, M.E., Bulen, C.L., Mertzman, S.L., Finegan, S.A., and McCleery, D.A., 2013, Intraplate magmatism related to opening of the Iapetus Ocean: Cambrian Wichita igneous province in the Southern Oklahoma rift zone: Lithos, v. 174, p. 57-70.

Harland, W.B., Armstrong, R.L., Cox, A.V., Craig, L.E., Smith, A.G., and Smith, D.G., 1990, A Geologic Time Scale 1989: New York, Cambridge University Press, 263 p.

Hogan, J.P., and Gilbert, M.C., 1995, The A-type Mount Scott Granite sheet: Importance of crustal magma traps: Journal of Geophysical Research, v. 100, p. 15779-15792.

Hogan, J.P., and Gilbert, M.C., 1997, Intrusive style of A-type sheet granites in a rift environment: The Southern Oklahoma Aulacogen, *in* Ojakangas, R.W., Dickas, A.B., and Green, J.C., eds., Middle Proterozoic to Cambrian Rifting, Central North America: Geological Society of America Special Paper 312, p. 299-311.

Hughes, S.S., McCurry, M., and Geist, D.J., 2002, Geochemical correlations and implications for the magmatic evolution of basalt flow groups at the Idaho National Engineering and Environmental Laboratory, *in* Link, P.K., and Mink, L.L., eds., Geology, Hydrogeology and Environmental Remediation, Idaho National Engineering and Environmental Laboratory, Eastern Snake River Plain: Geological Society of America Special Paper 353, p. 151-173.

Jean, M.M., Shervais, J.W., Champion, D.E., and Vetter, S.K., 2013, Geochemical and paleomagnetic variations in basalts from the Wendell Regional Aquifer Systems Analysis (RASA) drill core: Evidence for magma recharge and assimilation–fractional crystallization from the central Snake River Plain, Idaho: Geosphere, doi:10.1130/GES00914.1

Johnson, K.S., 1990, Geologic Map and Sections of the Arbuckle Mountains, Oklahoma, revision of Ham, W.E., McKinley, M.E., et al., 1954: Norman, Oklahoma, Oklahoma Geological Survey Map GM-31, scale 1:100,000.

Johnson, K.S., Amsden, T.W., Denison, R.E., Dutton, S.P., Goldstein, A.G., Rascoe, B., Jr., Sutherland, P.K., and Thompson, D.M., 1988, Southern midcontinent region, *in* Sloss, L.L., ed., Sedimentary Cover-North American Craton; U.S.: Boulder, Colorado, Geological Society of America, The Geology of North America, vol. D-2, p. 307-359.

Keller, G.R., and Stephenson, R.A., 2007, The Southern Oklahoma and Dnieper-Donets Aulacogens: A comparative analysis, *in* Hatcher, R.D., Jr., Carlson, M.P., McBride, J.H., and Martínez Catalán, J.R., eds., 4-D Framework of Continental Crust: Geological Society of America Memoir 200, p. 127-143.

Le Bas, M.J., LeMaitre, R.W., Streckeisen, A., and Zanettin, B., 1986, Chemical classification of volcanic rocks based on total alkali-silica diagram: Journal of Petrology, v. 27, p. 745-750.

Lofgren, G., 1971, Spherulitic textures in glassy and crystalline rocks: Journal of Geophysical Research, v. 76, p. 5635-5648.

McConnell, D.A., 1989, Determination of offset across the northern margin of the Wichita uplift, southwest Oklahoma: Geological Society of American Bulletin, v. 101, p. 1317-1332.

McPhie, J., Doyle, M., and Allen, R., 1993, Volcanic textures: A Guide to the Interpretation of Textures in Volcanic Rocks: University of Tasmania, Center for Ore Deposit and Exploration Studies, 196 p.

Miyashiro, A., 1974, Volcanic rock series in island arcs and active continental margins: American Journal of Science, v. 274, p. 321-355.

Pearce, J.A., Harris, N.B.W., and Tindle, A.G., 1984, Trace element discrimination diagrams for the tectonic interpretation of granitic rocks: Journal of Petrology, v. 25, p. 956-983.

Perry, W.J., Jr., 1989, Tectonic Evolution of the Anadarko Basin Region, Oklahoma: U.S. Geological Survey Bulletin 1866A, 19 p.

Price, J.D., Hogan, J.P., Gilbert, M.C., and Denison, R.E., 1998, Field guide to the basement rocks of the Southern Oklahoma aulacogen: Guidebook, South-Central Meeting of the Geological Society of America, March 20-24, Norman, Oklahoma, University of Oklahoma, 89 p.

Shelley, D., 1993, Igneous and Metamorphic Rocks under the Microscope: London, Chapman & Hall, 445 p.

Shervais, J.W., Vetter, S.K., and Hanan, B.B., 2006, Layered mafic sill complex beneath the eastern Snake River Plain: Evidence from cyclic geochemical variations in basalt: Geology, v. 34, p. 365-368.

Stitt, J.H., 1973, Biostratigraphy and depositional history of the Timbered Hills and Lower Arbuckle Groups, western Arbuckle Mountains, Oklahoma, *in* Ham, W.E., 1973, Regional Geology of the Arbuckle Mountains, Oklahoma: Oklahoma Geological Survey Special Publication 73-3, p. 19-23.

Sun, S.S., and McDonough, W.F., 1989, Chemical and isotopic systematics of oceanic basalts: Implications for mantle composition and process, *in* Saunders, A.D., and Norry M.J., eds., Magmatism in the Ocean Basins: Geological Society of London Special Publication No. 42, p. 313-345.

Thomas, W.A., Tucker, R.D., Astini, A.A., and Denison, R.E., 2012, Ages of pre-rift basement and synrift rocks along the conjugate rift and transform margins of the Argentine Precordillera and Laurentia: Geosphere, v. 8, p. 1366-1383.

Whalen, J.B., Currie, K.L., and Chappell, B.W., 1987, A-type granites: Geochemical characteristics, discrimination and petrogenesis: Contributions to Mineralogy and Petrology, v. 95, p. 407-419.

White, J.D.L., and Ross, P.-S., 2011, Maar-diatreme volcanoes: A review: Journal of Volcanology and Geothermal Research, v. 201, p. 1-29.

Williams, H., Turner, F.J., and Gilbert, C.M., 1982, Petrography: An Introduction to the Study of Rocks in Thin Section, 2nd Ed.: San Francisco, California, W.H. Freeman and Company, 626 p.

Winchester, J.A., and Floyd, P.A., 1977, Geochemical discrimination of different magma series and their differentiation products using immobile elements: Chemical Geology, v. 20, p. 325-343.